METHODS FOR THERMALLY BALANCED MOUNTING OF REFRACTIVE OPTICAL ELEMENTS

By

Nathan Wallace

A Master's Report Submitted to the Faculty of the

WYANT COLLEGE OF OPTICAL SCIENCES

In Partial Fulfillment of the Requirements

For the Degree of

MASTER OF SCIENCE

In the Graduate College

THE UNIVERSITY OF ARIZONA

2021

Table of Contents

1. Abstract

Thermal excursions pose a risk for performance degradation in optical systems. For refractive based systems, the thermal effects can change the focus of the system or cause unwanted stress within the optical elements. Mounting refractive elements in a way that minimizes the effects of thermal excursions will result in a system that will perform and survive over a wide range of temperatures. To accomplish this, methods that utilize spacer materials can be used to athermailize the axial load applied to an optical element. A spacer effectively compensates for the differential thermal expansion of the glass element and mechanical housing. For convex elements, the thermal growth of the spacer in the radial direction can be accounted for to ensure no loss of contact or high stress on the lens surface. Other methods include the design of athermalized RTV bonding between the outside diameter of the lens and the inside diameter of the housing, as well as compliant mounting methods. Finally, passive focus compensation can be accomplished by combining materials that will match the focal plane shift over temperature, ensuring the system remains focused during temperature changes. Thermally balanced systems employ many of these methods to achieve successful performance over wide operational temperature ranges.

2. Introduction

Refractive optical elements are major components of a wide variety of optical systems. These lens systems can be found almost everywhere, including cellphone cameras, medical devices, semiconductor equipment and high end space based systems. Each of these systems needs to be designed to satisfy the optical performance requirements over a wide variation in environmental conditions. One such environmental condition that has a profound effect on the performance of an optical system is temperature variation. Not only is temperature a concern for the optical design, but it also presents unique design challenges for the opto-mechanical engineer. With some careful design considerations, the opto-mechanical engineer can mitigate and potentially eliminate some of the adverse performance effects from these temperature variations. These design considerations take into account the thermal behavior of glass lenses, the effects of the mechanical interface to mount each lens and the trade space for system performance. The result of these design choices would be an opto-mechanical system design that is thermally balanced.

A thermally balanced opto-mechanical design is useful for optical systems that are required to perform over a wide temperature range or systems that may be thermally sensitive and require a high degree of optical performance. The thermally balanced design can mitigate issues such as changes in stress imparted on the lens, lens element movement and changes in the flange focal length over temperature.

Thermal balancing has been successfully used, for example, on the Multi-Angle Imaging Spectral Radiometer (MISR) for the TERRA Platform. This design includes thermally balanced focus compensation as well as individual compensators for the lens elements. The combination of these techniques allowed this system to achieve no detectable performance change over a temperature range of 0°C to 10°C [1]. The methods for thermally balancing and mounting refractive optics systems will be explored in this paper.

3. Thermal Effects of Refractive Glass

Optical glass is a carefully manufactured material that provides specific properties that are desirable for the propagation of light. Lens designers combine glasses with different core properties, i.e. index of refraction and abbe number, to carefully control optical aberrations and deliver a system that meets the desired performance requirements [2]. Although there are an impressive amount of parameters for each type of glass, particularly those properties for the use in optical design, only the pertinent properties that concern thermal effects will be considered to design a system that is thermally balanced. The vital thermal properties are the coefficient of thermal expansion (CTE) and thermal coefficients of refractive index

The CTE of glass, and many materials for that matter, is a coefficient that helps describe the dimensional change with temperature. Typical materials respond isotropically to temperature changes, that is, the value of the CTE is the same in all directions. Since the CTE is the same in all directions, the dimension change will also follow this behavior. This CTE value is generally reported as the change in linear size per unit length per degree of temperature. Table 1 shows some common materials their respective CTE values. Optical glass generally has a relatively low CTE compared to metallic materials. An even larger differential between CTEs can be seen with polymers, which can have values an order of magnitude or more than that of optical glasses. Table 2 shows an example from the datasheet for S-BSL7, where the thermal properties can be found [3].

MATERIAL	CTE (ppm/°C)	TYPE
PEEK	55.0	Plastic
Aluminum 6061	23.6	Metal
Stainless Steel 316	16.0	Metal
Titanium 6AL-4V	8.6	Metal
S-FPL53	14.5	Glass
S-BSL7	7.2	Glass
Fused Silica (7980)	0.57	Glass

TABLE 1. Common materials used in optical systems and their respective coefficient of thermal expansion in ppm/°C.

Thermal Properties		
Strain Point StP (°C)		532
Annealing Point AP (°C)		563
Transformation Temperature Tg (°C)		576
Yield Point At (°C)		625
Softening Point SP (°C)		718
Expansion Coefficients α (10^{-7}/°C)	(-30~+70°C)	72
	(+100~+300°C)	86
Thermal Conductivity λ W/(m·K)		1.13

TABLE 2. Thermal properties from Ohara S-BSL7 glass datasheet [3].

Looking at the CTE for glass can enable the opto-mechanical engineer some insight into how a lens element will behave with temperature. With elevated temperatures, the radius of curvature, the center thickness and the diameter will increase approximately linearly. The opposite dimensional changes occur with a decrease in temperature. For elements with a concave surface and an annulus, there will also be a change in the sagittal depth, or the SAG of the surface. If the annulus is used for mounting, then it will contribute to thermal changes in the airspace. These are considered geometric changes with temperature as the physical lens has changed dimensionally. Figure 1 shows the dimensional changes with temperature for a typical bi-convex lens.

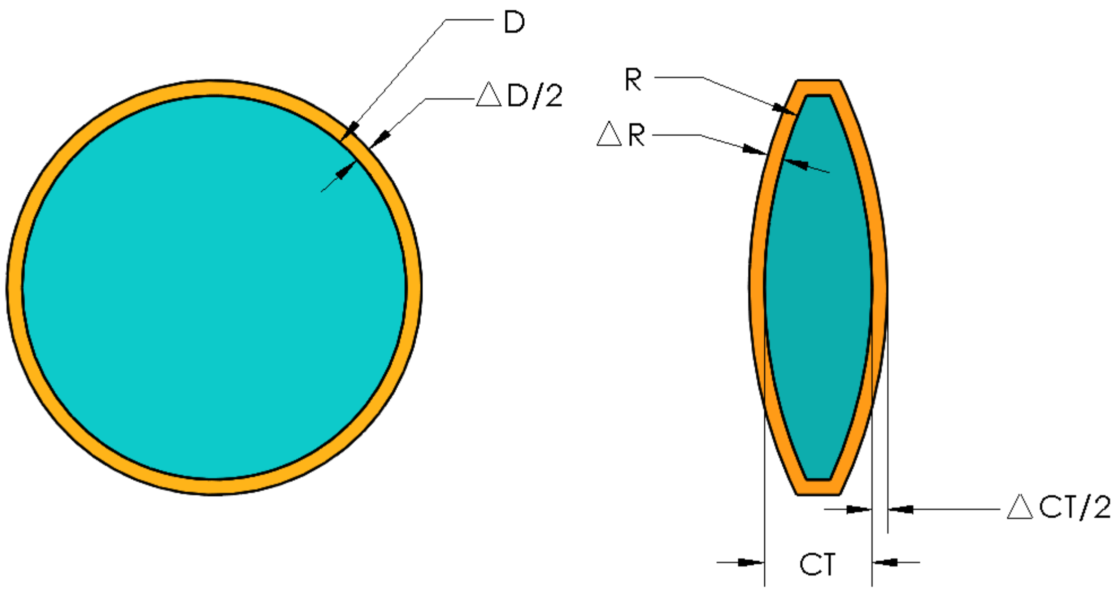

FIGURE 1. Dimensional changes with temperature for a typical lens. The original lens is colored blue and the orange shading shows the expansion with elevated temperature. R – radius of curvature, D – diameter, CT – center thickness.

Optical glasses will also exhibit a variation of index with temperature changes. This is a carefully characterized property and can be utilized by the optical engineer to ensure system performance over temperature. A change in the index of refraction for a lens, along with the dimensional changes described above can change how well a lens corrects for aberrations. Although the details of this behavior and the design approaches to help mitigate this effect will not be described here, it is worth some understanding for the opto-mechanical engineer to better appreciate the challenges faced by the optical engineer. This change in refractive index can be listed as a dn/dT, and with some understanding of geometrical optics can be converted into a change of focal length with temperature, df/dT. The change in focus over temperature is a concern for both the optical and opto-mechanical engineer.

The change in index with temperature dn/dT is referred to as the thermo-optic coefficient. It is very important to note that there are a few distinct and nuanced versions of the thermo-optic coefficient [4]. The first, and most common version, uses the relative index of the glass with respect to the index of air, dn_{rel}/dT. For applications where the surrounding medium is air and is expected to change temperature along with the glass, this is an appropriate model. The second version of the thermo-optic coefficient uses the absolute index of the glass with respect to vacuum. Equation 1 shows the relationship between the relative index change and the absolute change with temperature.

$$\frac{dn_{abs}}{dT} = n_{rel}\frac{dn_{air}}{dT} + n_{air}\frac{dn_{rel}}{dT} \qquad \text{Eq. (1)}$$

n_{abs} = Index relative to vacuum
n_{air} = Index of air
$n_{rel} = n_{abs}/n_{air}$
T = Temperature

The relative thermo-optic coefficient is useful in cases where the optical system undergoes a uniform and steady-state temperature change. In other cases, such as differences in air temperature with respect to the optical system, or systems experiencing different thermal loads like a thermal gradient, the use of the absolute thermo-optic coefficient is the better choice [4].

The thermo-optic coefficient is a useful property of refractive materials and can be readily converted into an even more useful equation, the change in focus with temperature of a lens. Equation 2 shows the change in focal length for a thin lens experiencing a steady-state temperature change. An important term can be collected in Equation 2, known as the opto-thermal expansion coefficient, shown in Equation 2a [4]. Figure 2 shows the change in focus for a simple lens experiencing a steady state temperature change.

$$\Delta f = \left[\alpha - \left(\frac{1}{n-1}\frac{dn_{rel}}{dT}\right)\right] f\Delta T \qquad \text{Eq. (2)}$$

n = Index of refraction of glass
f = Focal length
α = Coefficient of thermal expansion (glass)

$$\eta_s = \left[\alpha - \left(\frac{1}{n-1}\frac{dn_{rel}}{dT}\right)\right] \qquad \text{Eq. (2a)}$$

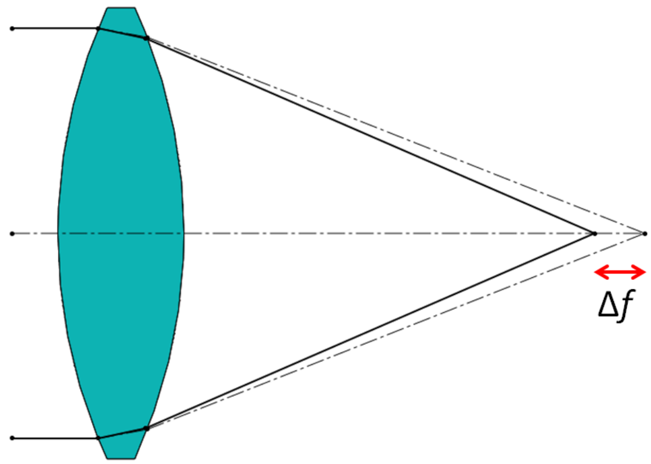

FIGURE 2. Change in focal length of a simple lens experiencing a steady state temperature change.

Understanding of how optical glass behaves with temperature can be used to inform the opto-mechanical design. Specific design choices can be made based on the performance needs of the system and the temperature extremes that it may have to operate over. Once the characteristics of the specific optical design have been define, the opto-mechanical engineer can start to look at ways to mount and secure the lens elements in a thermally benign way. These mounting methods are described in Sections 5, 6 and 7. The thermal focus change can be compensated for by the opto-mechanical design and methods are explored in Section 8.

4. Lens Mounting and Thermal Effects

There are many different approaches to mounting optical lenses. It is important to understand the different mounting methods of lenses before starting the process of analyzing how they respond to thermal changes. One of the most cost effective and easily assembled methods is the use of threaded retaining rings. [5] Figure 3a shows a lens mounted with a threaded retaining ring. The lens can contact the threaded retainer directly, or lens spacers can be employed to act as the lens to mechanical interface.

Contacting the curved optical surfaces of a lens element will create component forces that will constrain the lens in the axial and radial directions. These component forces are a result of an axial preload applied to the lens as well as the curvature of the optical surface. Figure 3b shows the component forces when an axial load is applied to a lens from a circular retainer. The relative magnitude of the component forces is dependent on the curvature of the surface. Interfacing directly with the optically polished and generally spherical surfaces provides many advantages with mounting [5], including that the component forces will generally balance to assist in centering the surface as the axial load is applied. The amount of axial load that is required to hold a lens in place is directly related to the weight of the lens, the tangent angle developed between the contacts and the coefficient of friction between the lens and the mechanical interfacing material [5]. Equation 3 shows this preload with the addition of a radial acceleration factor applied to the weight. This general form of the equation can be used to solve for a preload to hold a lens in place when subjected to an amount of radial acceleration, a_0 [5].

There are a few contact types that can be utilized on spherical lens surfaces when considering mounting methods like retainers and spacers. These contact types are the sharp corner contact, the tangent contact and a spherical contact. Each contact type will require the same preload as shown below, in Equation 3, to properly secure the lens in place.

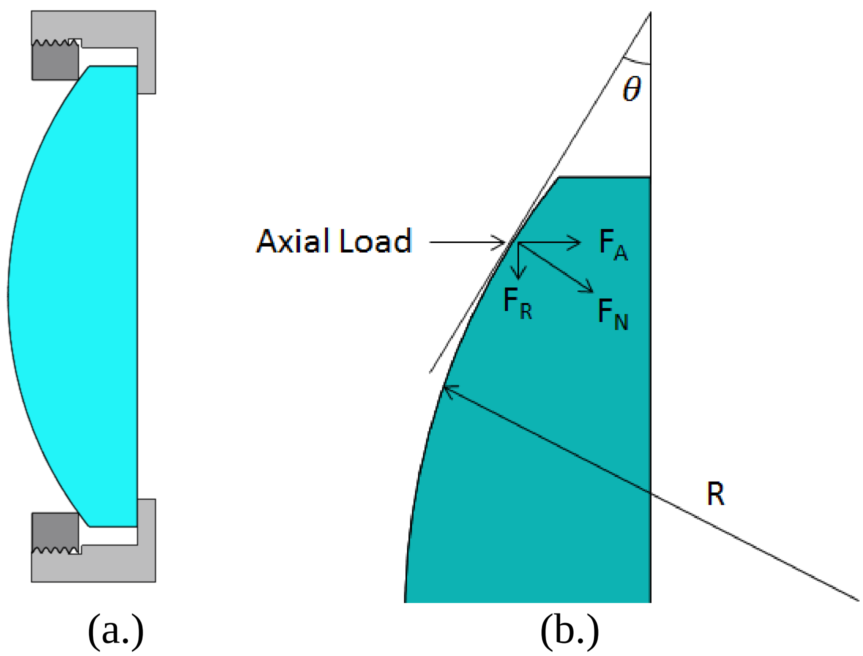

FIGURE 3. (a) A lens held in place with a threaded retaining ring. (b) Cross section of a lens showing component forces generated when an axial load is applied to a convex spherical surface. F_A – force in the axial direction, F_N – force normal to the surface, F_R – force in the radial direction, R – radius of curvature, θ – total included tangent angle.

$$P = \frac{W a_0}{\mu_S} \cos^2 \theta \qquad \text{Eq. (3)}$$

W = Weight of the lens
a_0 = Radial acceleration as a factor of gravity
μ_S = Coefficient of static friction
θ = Total included tangent angle

The sharp corner interface represents the simplest instantiation of axial retention. Here a spacer or retaining ring is simply a ring with a square cross section. Figure 4a shows a lens mounted with a sharp corner. The inside diameter of the spacer is sized so as to not occlude the optical light path and the outside diameter is sized to fit within the lens barrel. This interface produces a circumferential line contact against the surface of the optic [5]. These sharp corner contacts are not truly sharp when they are machined. Surfaces that have been processed with proper de-burring result in a corner with a radius on the order of 50 microns [5].

The tangent interface is where a tangent cone interfaces with the spherical lens surface. Figure 4b shows a lens mounted with a tangent spacer. The half angle cone can be found using Equation 4 The tangent spacer is a near ideal interface for a spherical surface and represents a balance between performance and manufacturability. The tangent contact has a remarkable reduction in stress when compared to the sharp corner contact [5]. The stresses will be explored later in this section.

$$Half\ Cone\ Angle = 90° - \sin^{-1}\frac{y_c}{R} \quad \text{Eq. (4)}$$

y_c = Radial height of contact at the lens surface
R = Radius of curvature of the lens

The spherical interface is another method to mount lens elements. This type of mount relies on the matching of the contact area to the radius of curvature of the lens element. It is important that the radii be matched very closely, usually by lapping, or the contact may quickly devolve into a sharp corner contact. This method of lens mounting has the advantage of the lowest stress but can be expensive compared to the sharp corner or tangent interface. Figure 4c shows the spherical interface.

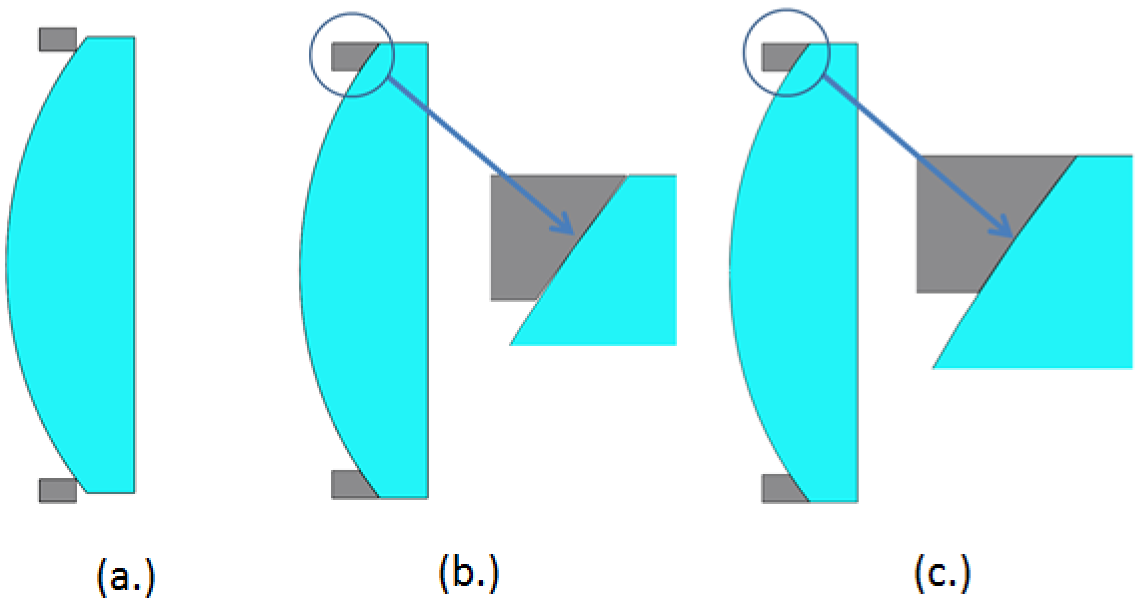

FIGURE 4. (a.) Sharp corner spacer interfacing with a convex lens surface. (b.) Tangent spacer interfacing with a convex lens surface. The tangent surface is a close approximation of the convex surface. (c) Spherical spacer interfacing with a convex lens surface. The ideal spherical surface of the spacer matches the lens surface radius of curvature perfectly.

An important aspect for determining the type of mounting method is reducing the stress imparted on the optical element. The method for determining the appropriate contact type varies significantly for a given particular system, however, it is critical to determine the stress imparted onto the optical element to ensure the chosen solution is appropriate. These stresses can impact the optical performance as well as create a threat to the failure of the optical element. Each mounting type has a convenient closed from solution for determining the stress in the lens element.

The stress developed in the sharp corner interface can be determined with Equation 5. This represents the peak compressive stress, S_c, at the line contact created by the sharp corner retainer or spacer. Equation 5a shows the K1 term and Equation 5b shows the K2 term. For the sharp corner interface specifically, a fixed value of 10/mm can be used for K1 where the small error from this approximation is less than 2% [2]. This assumption can be made for conditions where D1 << D2, assuming the sharp corner has a radius of 50 microns.

Similar to the sharp corner interface, the peak compressive stress, S_c, can be calculated using Equation 5c for the tangent spacer. In this case the K1 term can be approximated as 1/D1, due to the infinite radius of the tangent contact. With this K1 term, the stress is significantly less than the sharp corner interface. Finally, the spherical contact stress can be determined rather trivially as the preload divided by the annular contact area [5]. This solution assumes the very close matching of the spherical surface of the spacer to the surface of the lens.

$$S_c = 0.798\left(\frac{K_1 p}{K_2}\right)^{1/2} \qquad \text{Eq. (5)}$$

p = preload per unit length of line contact

$$K_{1\,(SHARP)} = \frac{D_1 + D_2}{D_1 D_2} \qquad \text{Eq. (5a)}$$

D_1 = 2*(Radius of curvature of the lens)
D_2 = Diameter of the sharp corner

$$K_2 = \frac{1-\nu_G^2}{E_G} + \frac{1-\nu_M^2}{E_M} \qquad \text{Eq. (5b)}$$

ν_G = Poisson's ratio of the glass
ν_M = Poisson's ratio of the metal
E_G = Modulus of elasticity (glass)
E_M = Modulus of elasticity (metal)

$$K_{1\,(TANGENT)} = \frac{1}{D_1} \qquad \text{Eq. (5c)}$$

D_1 = 2*(Radius of curvature of the lens)

An important component of determining the maximum stress allowed in many optical elements is that the tensile stress developed at the contact interface will be the limiting stress. This is generally true for brittle materials such as optical glass. Figure 5 shows the tensile regions of a Hertzian contact on a lens surface [6]. The tensile component of a Hertzian contact can be determined by Equation 6. For simplified calculations the relationship of compressive stress to tensile stress can be estimated by dividing the compressive stress by 6. This ratio of $\sigma_{Tensile}=\sigma_{Compressive}/6$ is a 1st order general rule that can be effectively applied to most situations. An additional simplification is that most optical glasses will fail around 6.9MPa – 10.3MPa of tensile stress. Using 6.9MPa as the tensile limit is generally an appropriate and conservative value [5]. Equation 6 should be used to calculate the tensile stress and an appropriate analysis for a particular glass tensile stress limit should also be used to achieve the most accurate values.

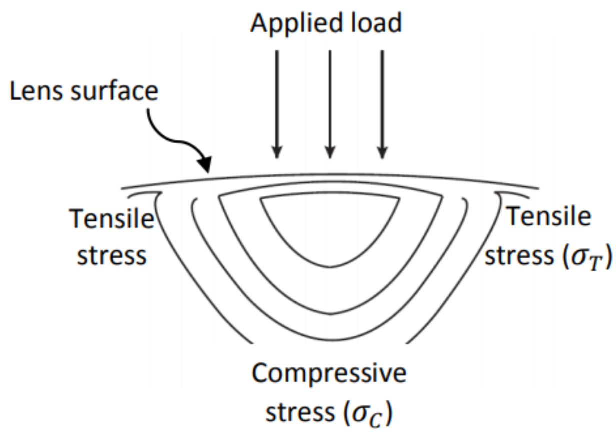

FIGURE 5. Tensile stress region for a Hertzian contact of an applied compressive load on a lens surface [6].

$$\sigma_T = (1 - 2\upsilon_G)\frac{\sigma_C}{3} \quad \text{Eq. (6)}$$

υ_G = Poisson's ratio of the glass
σ_C = Compressive stress

Figure 6 shows the tensile stress as a function of interface radius. The assumptions are a 100N axial preload for an S-BSL7 lens of radius of curvature of 50mm and a spacer made from 6061 aluminum. It is useful to note the large stress factor difference between the sharp corner interface and the tangent interface, where the stress of the tangent contact in invariant due to the infinite radius and the sharp corner varies as a function of the contact radius. As the radius of the sharp corner becomes very large, the contact starts to match the stress from the tangent interface. In this particular case, the sharp corner contact is above the conservative 6.9MPa tensile limit and would not be advised for this design.

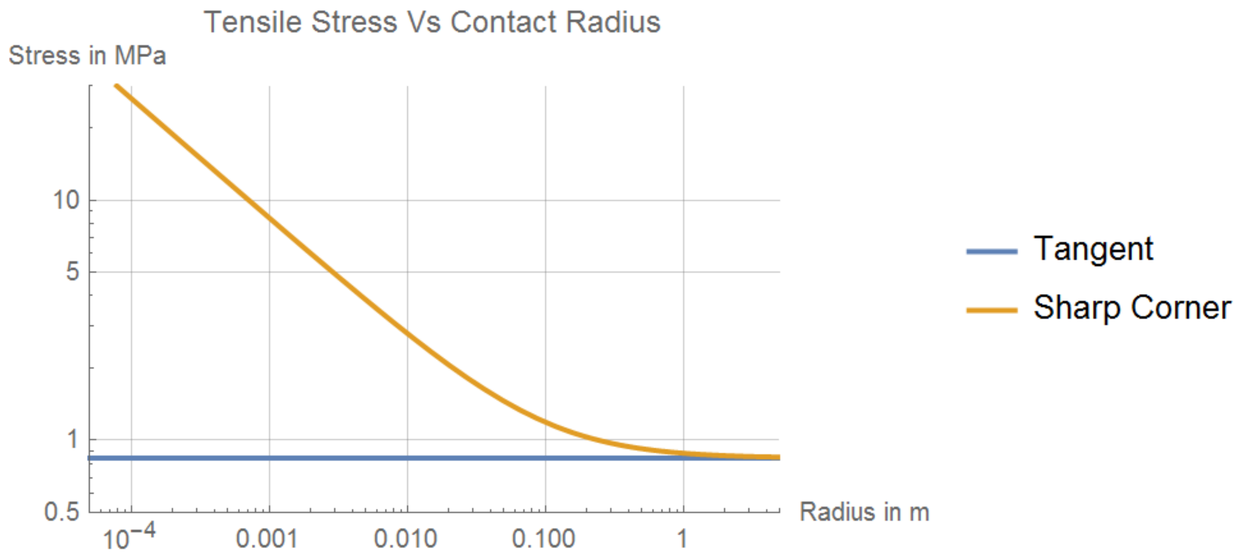

FIGURE 6. Plot showing the tensile stress versus contact radius of a sharp corner and tangent interface.

Based on the design of the traditional mounting methods above, the effect of temperature on the loading and constraint of the lens can be analyzed. Lens elements and their respective housings, generally speaking, will have differing CTEs. This difference in CTE presents a challenge to the opto-mechaincal engineer to be able to provide sufficient mounting forces over thermal excursions. Consider a glass lens element with a comparatively low CTE than its metallic housing. As temperature increases, the housing will grow by a dimension defined by its CTE and the change in temperature. The optic, having a lower CTE, will also experience a change in dimension with temperature, but this change will be much less in magnitude than that of the housing. At some temperature, $T_{Critical\text{-}High}$, the retainer will no longer be in contact with the lens element. Figure 7 shows the initial temperature with the lens held in place and the elevated temperature where the retainer has lost contact with the lens. This critical temperature can be approximated by Equation 7 [5].

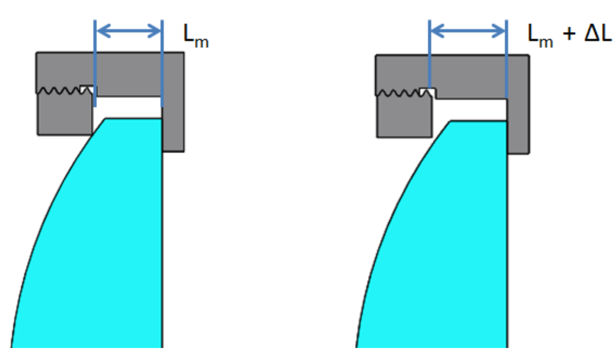

FIGURE 7. The critical temperature, $T_{Critical\text{-}High}$, where the differential expansion of the lens barrel causes the retainer to lose contact with the lens surface.

$$T_{Critial-High} = T_A - \frac{P_A}{K_3} \qquad \text{Eq. (7)}$$

P_A = Axial preload at assembly
K_3 = Preload rate of change
T_A = Temperature at assembly

Likewise, with a decrease in temperature, the housing will dimensionally shrink faster than the lens and result in an increase in the axial preload applied to the lens element. At some $T_{Critical\text{-}Low}$ the stress imparted on the optic will be high enough to cause the glass to fracture.

The equations presented above assume that the housing will have a higher CTE than the lens elements. In some cases this may not be true and the critical temperatures will need to be reversed. Some examples include the use of plastic lens elements, such as PMMA in a metal housing or glass elements in an invar housing. In these cases, the high temperature results in the increased loading and the low temperature results in the release of loading.

The variations in loading, specifically the axial preload of a lens over a temperature change, can be approximated by using Equation 8. The preload rate of change, K3, can be found using Equation 8a. For the A_G term, if $(2y_C+t_E) \leq D_G$ then Equation 8b should be used. If $(2y_C+t_E) > D_G$ then Equation 8c should be used. This relationship comes from the area of the stressed region inside the lens and whether or not it is contained within the lens rim or truncated by it [5]. Equation 8d can be used to find the stressed region in the housing. Figure 8 shows the preload change for a simple S-BSL7 lens mounted in an aluminum housing where y_C=12mm, t_E=4mm, t_C=2mm, D_G=25mm. Even in this relatively simple case, the preload change with temperature is significant. This rate of preload change can become alarming for multiple elements loaded in a lens barrel. There is a design balancing act to maintain an appropriate preload at elevated temperatures to prevent radial alignment changes of the lens elements and stress levels imparted on the optic at low temperatures to prevent failures. The most striking and often overlooked outcome of the axial preload change in temperature is the potential performance degradation from stressing the optical element. The impact of stresses to system performance needs to be looked at for each application but can be very problematic for systems where there is very little performance margin between the performance requirements and the diffraction limit.

$$P = K_3 \Delta T \qquad \text{Eq. (8)}$$

P = Change in preload for a given temperature
K_3 = Preload rate of change

$$K_3 = \frac{-(\alpha_M - \alpha_G)t_E}{\frac{2t_E}{E_G A_G} + \frac{t_E}{E_M A_M}} \qquad \text{Eq. (8a)}$$

E_G = Modulus of elasticity (glass)
E_M = Modulus of elasticity (metal)
t_E = Axial thickness of the material at the contact location
α_M = CTE (metal)

α_G = CTE (glass)
A_G = Area of the stressed region in the lens
A_M = Area of the stressed region in the housing wall

$$A_G = 2\pi y_C t_E \qquad \text{Eq. (8b)}$$

y_c = radial height of contact

$$A_G = \frac{\pi}{4}(D_G - t_E + 2y_C)(D_G + t_E - 2y_C) \qquad \text{Eq. (8c)}$$

D_G = Diameter of the lens

$$A_M = \pi t_C (D_M + t_C) \qquad \text{Eq. (8d)}$$

t_c = Housing wall thickness at the lens rim
D_M = Inside diameter of the housing at the lens

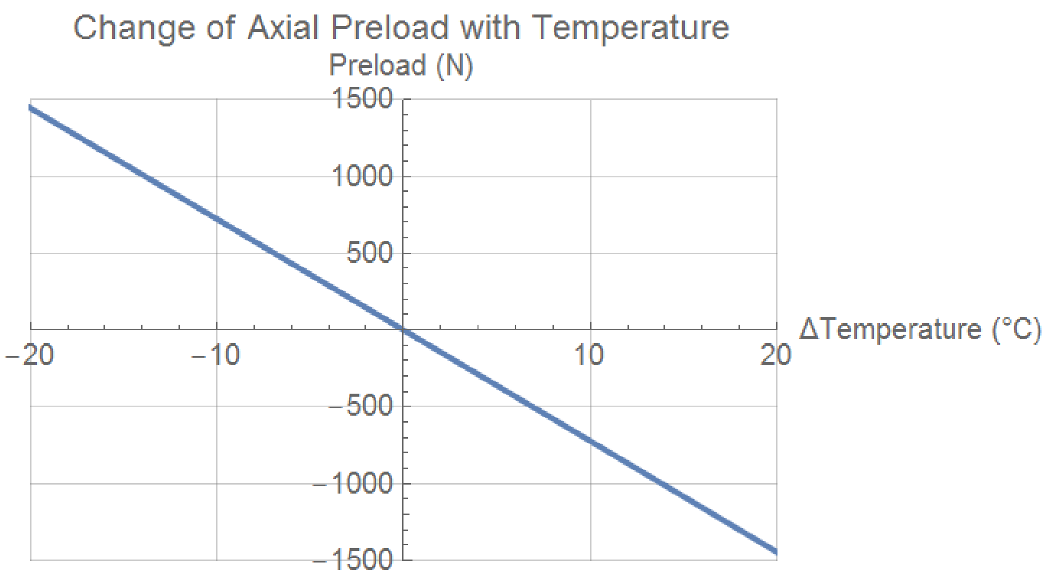

FIGURE 8. Plot of the axial preload change for a lens made from S-BSL7 and an aluminum housing over a temperature change of +/- 20°C.(y_C=12mm, t_E=4mm, t_C=2mm, D_G=25mm)

An often overlooked effect of stress on optical glass is on the birefringence of the material. Birefringence is a difference in the refractive index of the glass in two orthogonal directions [7]. When stresses are applied to an optical glass, the magnitude of the birefringence can change based on the stress. This is referred to as stress induced birefringence. For applications that involve the use of polarized light, this effect can degrade the performance of the system. Equation 9 can be used to determine the stress birefringence [7]. The value K is known as the stress optic coefficient or sometimes called the photoelastic constant (β) and can be found in the manufactures properties for optical glass. A useful formula to calculate the change in optical path difference when a component is stressed is shown in Equation 10.

$$\Delta n = K(\sigma_1 - \sigma_2) \qquad \text{Eq. (9)}$$

K = Stress optic coefficient
σ_1,σ_2 = Principal stresses in the orthogonal axes to the propagation direction

$$\Delta OPD = \Delta n t \qquad \text{Eq. (10)}$$

t = Material thickness

5. Axial Preload Compensator Design

With careful design and analysis, the axial loading effects from temperature can be significantly mitigated for mounted lenses in optical systems. The application of materials with complimentary thermal properties can compensate for the axial changes experienced with thermal excursions. The benefit of this axial compensation is the reduction of stress imparted on the optical element and the ability of the optical element to remain aligned and in contact with the mechanical mounts over a wide range of temperatures.

In order to explore the various methods of thermal balancing it is important to have a list of materials that can be used for this purpose. Table 3 gives a list of various materials that can be successfully used to provide axial thermal compensation. This list is in no way the only materials that can be used, but rather provides some general guidance for approaching the design. Other design requirements or factors may preclude or eliminate some of these materials over others. In these cases, the appropriate choice will be based on the needs of the system. In addition to the desirable thermal properties, and particularly for optical applications, it is important that materials be compatible with optics. Outgassing can be a significant deciding factor when choosing a polymer based solution. Thus, finding polymers that adhere to the NASA low outgassing guidelines would almost always be a wise choice. In order for a material to pass the NASA guidelines it must have a total mass loss (TML) of less than or equal to 1.0% and a collected volatile condensable materials (CVCM) of less than or equal to 0.10% [8].

MATERIAL	**CTE (ppm/°C)**	**CTE (ppm/°F)**
PEEK	45.0	25
Celazole U-60	23.4	13
Duratron CU 60 PBI	23.4	13
ETFE Tefzel	131.4	73
PCTFE (Kel-F)	126.0	70
Semitron 500HR PTFE	102.6	57
Techtron PPS	50.4	28
Torlon 4203	30.6	17
Ultem 1000	55.8	31
Vespel SP-1	54.0	30

TABLE 3. List of compensating spacer materials and their relevant CTEs. Materials pass NASA outgassing requirements per ASTM-E595 [9]

The method for designing an axial thermal compensator starts with collecting all of the materials that are in the structural loop around the lens in the axial direction. Consider the simple case shown in Figure 9. Here a bi-concave singlet lens is mounted in a barrel and held in place with a retainer interfacing with the flat bevel of the lens. Now consider the various thermal cases of this same mounted lens in Figure 10. Due to the differences in the coefficient of thermal expansion (CTE) between the lens and the housing, the axial load applied to the lens will also vary. This was shown in the previous section and is referred to as the temperature sensitivity factor K3 [5]. Equations 11, 12 and 13 are the change in length at the point of contact for each component, the metal housing (m), the spacer (s) and the glass elements (g) which can be used to solve for this dimensional change. α is the CTE for the material, l is the length of the materials and ΔT is the change in temperature. With the addition of a spacer made from a thermally complimentary material, the axial dimensional changes from temperature can be eliminated.

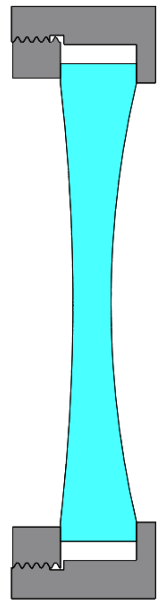

FIGURE 9. A bi-concave lens shown mounted with a retaining ring.

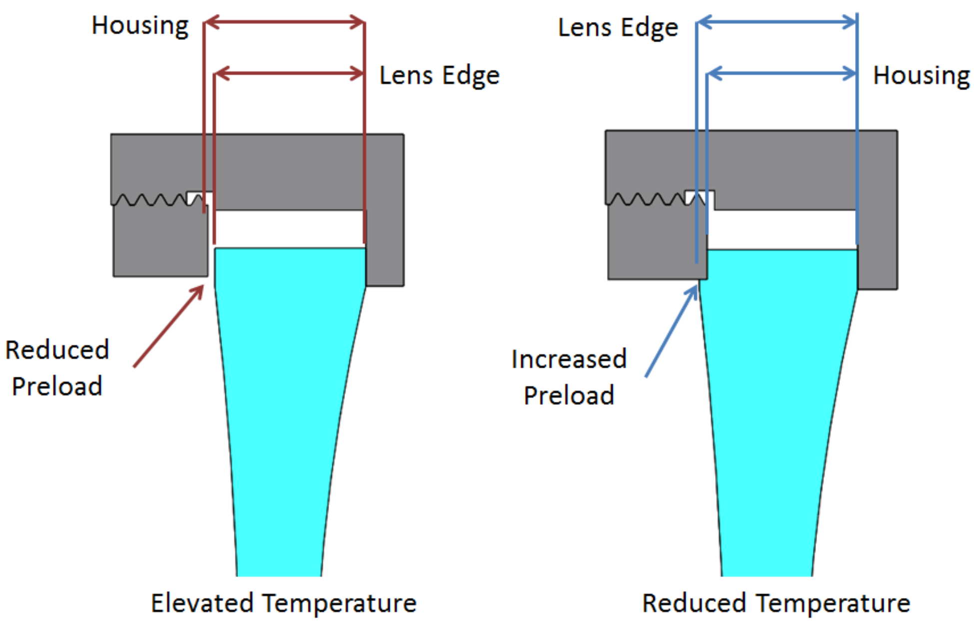

FIGURE 10. Thermal cases for a bi-concave lens mounted in a metal housing. At elevated temperatures the housing dimensionally expands more than the glass lens causing a reduction in axial preload. At reduced temperatures the housing dimensionally contracts more than the glass lens causing an increase in axial preload.

$$\Delta l_m = l_m \alpha_m \Delta T \qquad \text{Eq. (11)}$$

$$\Delta l_g = l_g \alpha_g \Delta T \qquad \text{Eq. (12)}$$

$$\Delta l_s = l_s \alpha_s \Delta T \qquad \text{Eq. (13)}$$

The ideal length of the compensating spacer can be found using Equation 14 which combines and solves Equations 11, 12 and 13 above [1]. With the addition of the compensating spacer to thermally balance the lens, the loading does not change over various thermal cases shown in Figure 11.

$$l_s(\alpha_s - \alpha_m) = l_g(\alpha_m - \alpha_g) \qquad \text{Eq. (14)}$$

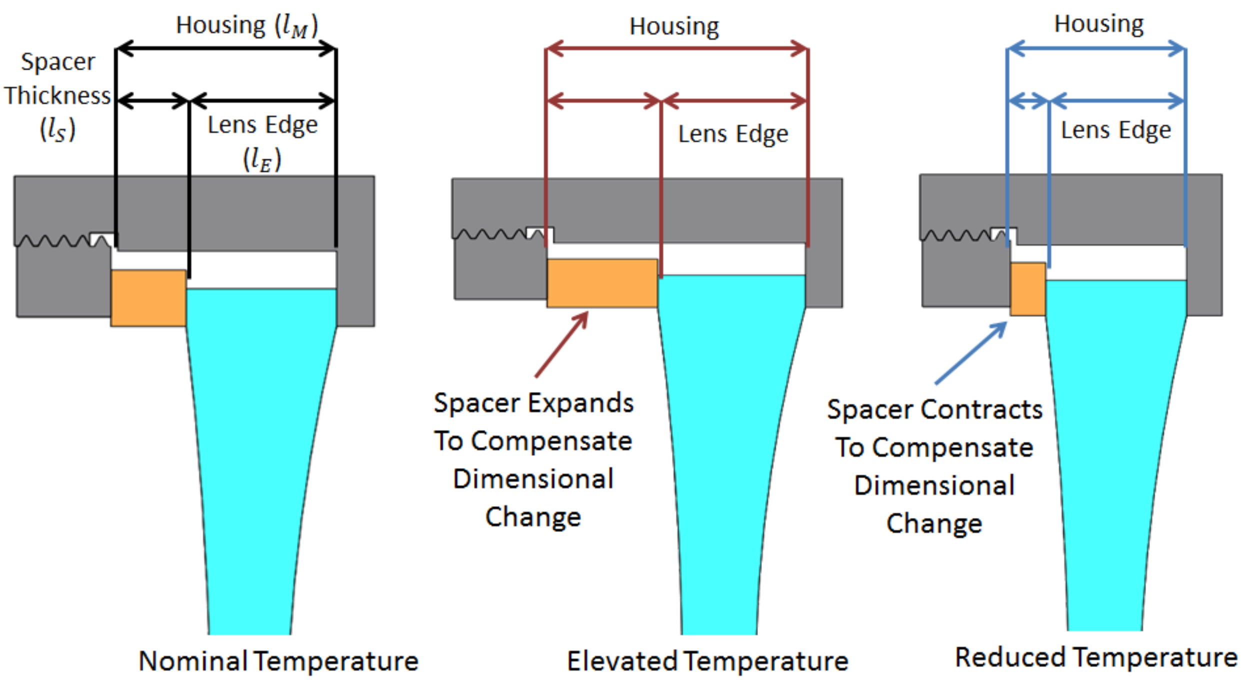

FIGURE 11. Thermal cases for a glass lens mounted in an aluminum housing. The compensating spacer thickness is designed to compensate the differential dimensional changes experienced by thermal changes of the cell.

A general expression for the axial compensation equation can be derived by looking at the contribution of each component to the change in length based on the CTE of the material and the change in temperature. Equation 15 shows the general form to calculate the ideal compensator length for an arbitrary stack of components. Since the length of the compensating spacer is not known in this example, the component equations can be combined and solved to find the required spacer length. The change in temperature, ΔT, conveniently cancels out. If the spacer thickness is known then this process can be used to solve for other parameters such as the length of the barrel or the glass element. Although this approach would be rare, it can occur when retrofitting an existing design with new components, where changes to the dimensions or the material of the spacer may not be possible.

$$l_s(\alpha_s - \alpha_m) = \sum_{i=1}^{n} l_i(\alpha_i - \alpha_m) \qquad \text{Eq. (15)}$$

A stack of multiple elements and spacers shown in Figure 12 can also be considered. Expanding the general form of the axial compensation shown in Equation 16 can be used to solve the required spacer length to compensate the entire stack.

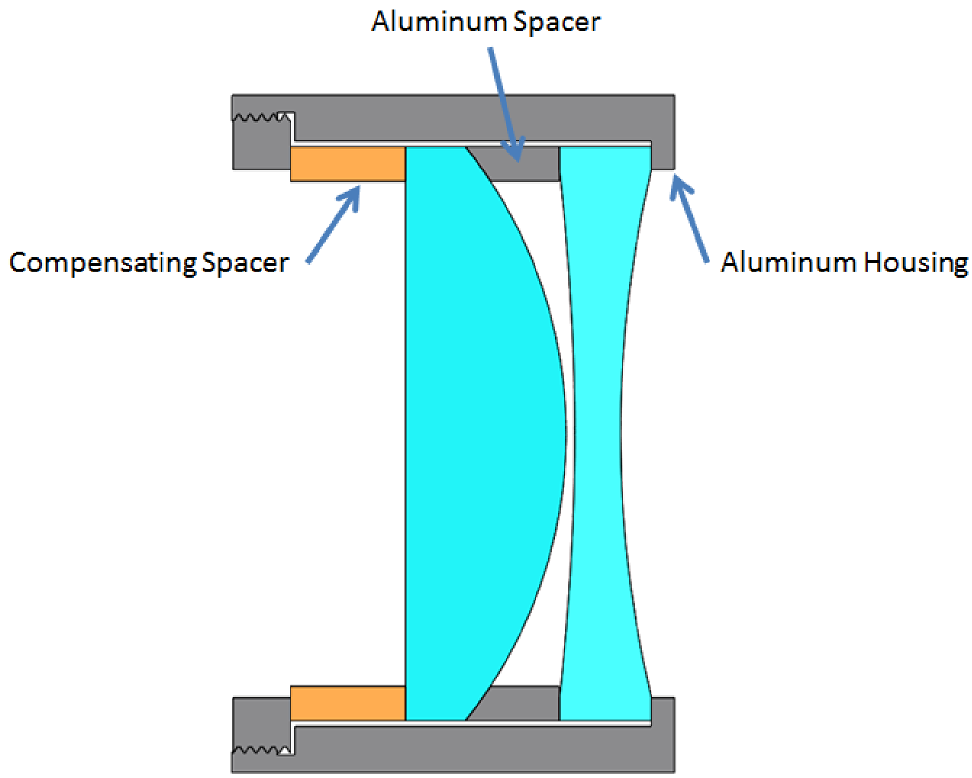

FIGURE 12. Multiple lenses in a stack can also be thermally balanced for axial preload by using a compensating spacer.

5.1 EXAMPLE: Axial Preload Compensator

With the basic set of equations previously detailed, a design example for bi-concave lens can be explored. Figure 13 shows a cross section of the starting design. The materials, dimensions and calculated spacer designs are summarized in Table 4.

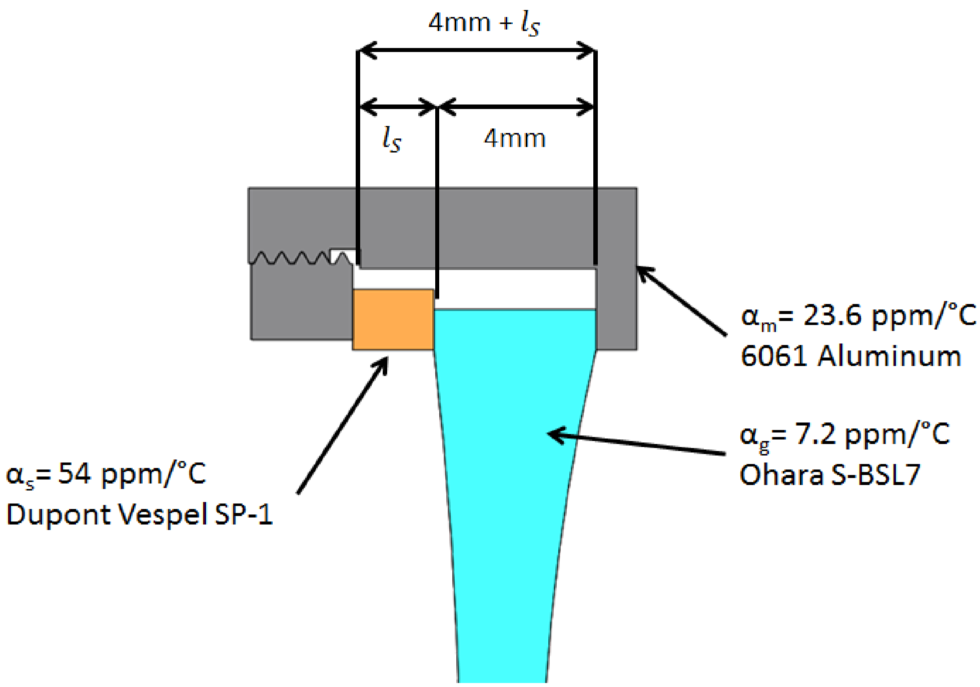

FIGURE 13. Cross-section of the starting design dimensions of the components required to find the ideal length of the axial compensating spacer.

Component	Length (mm)	CTE (ppm/°C)	Material
Lens	4	7.20	S-BSL7
Housing	6.16	23.6	6061
Spacer	2.16	5.40	Vespel SP-1

TABLE 4. Summary of the dimensions, materials and CTEs used for the example spacer design. The ideal spacer length was found to be 2.160mm.

5.2 Axial Preload Radial Effects

The example presented above will work well for lenses with plano surfaces, but is only an approximation for use with spherical lens surfaces. A spherical surface will have a component of the compensation in the axial direction as well as the radial direction. The interaction of the radius of curvature for the surface and the radial dimensional change with temperature of the compensating spacer needs to be quantified. Equation 16 is the change in change in radius of the optical surface with temperature and Equation 17 can be used to calculate the diametral change in the spacer size with temperature. Figure 14 shows the changes both axially and radially as temperature is increased. Combining these effects produces a more accurate formula for evaluating and designing thermal balancing spacers. The sagitta, or SAG of the surface can be calculated using Equation 18. This is distance from the vertex of the lens to the point of contact at some radial height. For spacer CTEs that are higher than the glass CTE and interfacing with convex surfaces, this value should be positive and for concave surfaces it should be negative.

However, additional analysis may be required in cases where the boundary conditions change for the spacer, lens or housing. In cases where there is a relatively small radial gap between the spacer in the lens housing, there will be a temperature where the spacer contacts and is constrained by the housing. In these cases the dimensional response to temperature is no longer solely defined by the CTE of the material and the strain in the spacer or housing needs to be incorporated in the model. At this point the finite element method would be the appropriate analysis path.

$$\Delta R = R\alpha_G \Delta T \qquad \text{Eq. (16)}$$

$$\Delta y_c = y_c \alpha_S \Delta T \qquad \text{Eq. (17)}$$

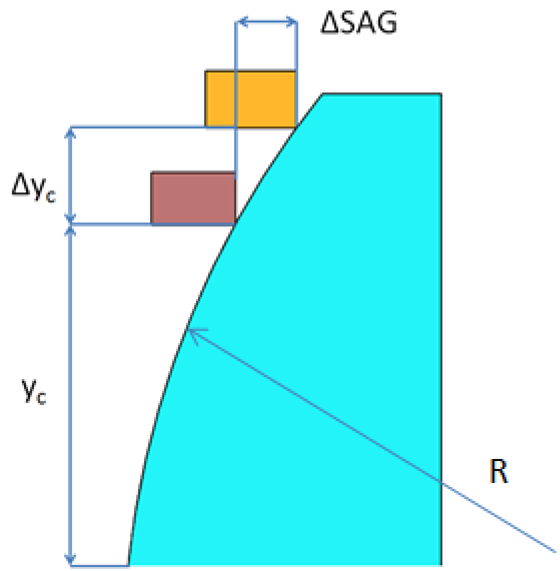

FIGURE 14. Cross-section of a lens segment showing the change in contact both radially and axially along a convex lens surface.

$$SAG = R - \sqrt{R^2 - {y_C}^2} \qquad \text{Eq. (18)}$$

R = Radius of curvature of the lens
y_c = radial height of contact

The quantity ΔSAG can be found by looking at the difference between the nominal SAG value and the SAG for a given temperature, SAG*. Equation 19 shows the formula for SAG* where the thermal change in radius, Equation 16, and the thermal change in yc, Equation 17 have been combined. The yc value has a contribution from the spacer CTE as well as the glass CTE, thus it can be calculated as the difference between the two values. The ΔSAG can be calculated with Equation 20. It is very convenient that the SAG over temperature is linear. This simplifies the closed form solution to find the ideal spacer thickness for compensating the axial preload. Figure 15 is a plot of the SAG vs. temperature for a 50mm radius lens with a yc of 12mm. Finally, the closed form solution can be found using Equation 21 and simplifying by taking the per unit degree from of ΔSAG by setting the ΔT=1°C.

$$SAG^{*} = (R + R\alpha_G \Delta T) - \sqrt{(R + R\alpha_G \Delta T)^2 - (y_C + y_C(\alpha_S - \alpha_G)\Delta T)^2} \quad \text{Eq. (19)}$$

R = Radius of curvature
y_c = radial height of contact
ΔT = Change of temperature
α_M = CTE (metal)
α_G = CTE (glass)
α_S = CTE (spacer)

$$\Delta SAG = SAG - SAG^{*}$$

$$= R\alpha_G \Delta T - \sqrt{R^2 - y_C^2} + \sqrt{(R + R\alpha_G \Delta T)^2 - (y_C + y_C(\alpha_S - \alpha_G)\Delta T)^2}$$

Eq. (20)

$$\approx \left(R\alpha_G - \frac{R^2\alpha_G - y_C^2(\alpha_S - \alpha_M)}{\sqrt{R^2 - y_C^2}} \right) \Delta T$$

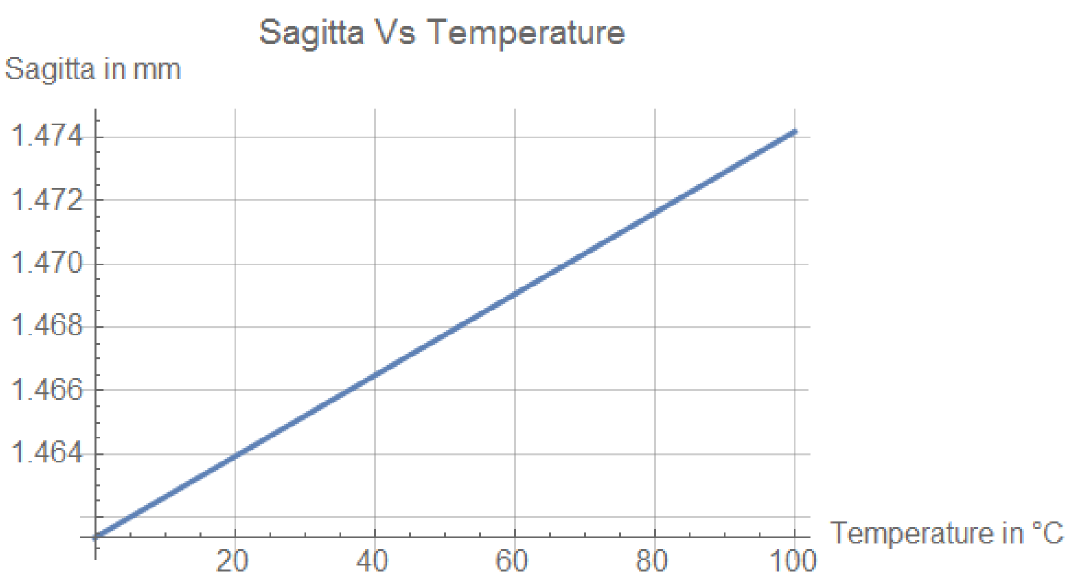

FIGURE 15. Plot of the SAG vs Temperature showing that the change in SAG is linear.

$$L_s = \frac{L_G(\alpha_M - \alpha_G) + \Delta SAG}{(\alpha_S - \alpha_M)} \qquad \text{Eq. (21)}$$

5.3 EXAMPLE: Axial Preload Compensator with Radial Effects

An example of a mounted convex lens can be explored to produce a thermally balanced axial preload. Assume a 25mm diameter convex lens with a radius of curvature of 50mm made from S-BSL7. The CT of the element is 7mm. The spacer contacts the element at a diameter of 24mm (12mm y_C height) and is made from Vespel SP-1. Figure 16 shows a cross section of the lens and spacer used in this example. This problem can be solved using Equation 14 as well as taking into account the SAG change with temperature from Equations 21. Table 5 shows the components, the material properties and the design dimensions using the method without the radial effects. The housing expansion is subtracted from the sum of the lens and spacer expansion. The ideal spacer thickness is 2.988mm when assuming no radial effects.

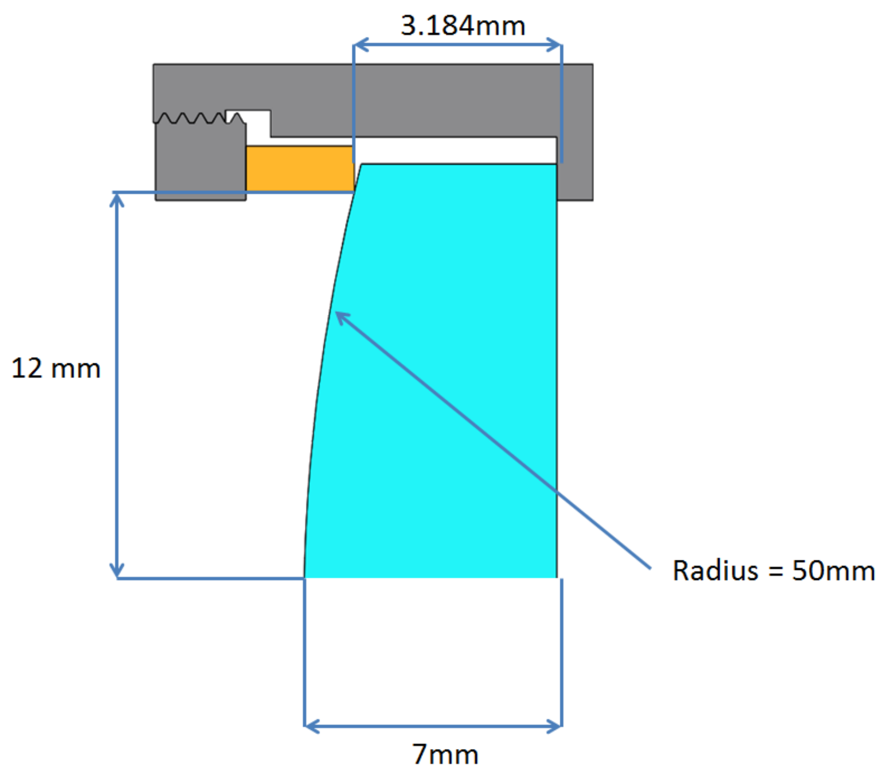

FIGURE 16. Cross-section of the lens and dimensions used for the example using only axial effects with temperature.

Component	Material	Bulk CTE (ppm/°C)	Length (mm)	ΔL/°C (mm)
Lens	S-BSL7	7.20	5.5386	3.99E-05
Spacer	Vespel SP-1	5.40	2.9880	1.61E-04
Housing	6061	23.6	8.5266	2.01E-04
		Expansion Difference		**0.0000**

TABLE 5. Summary of the materials, dimensions and total differential expansion for the axial compensator design without radial effects. The ideal length of the compensating spacer in this case is 2.998mm.

Now the same example can be evaluated using the radial effects. Table 6 shows the calculation for the starting ΔSAG per unit °C. Using this data and inputting it in Equation 29, the ideal spacer can be found to be 7.199mm. The sign of ΔSAG depends on the type of lens surface that the spacer is interfacing with. With a convex surface the ΔSAG causes an axial increase with temperature and with a concave surface causes an axial decrease with temperature. The inclusion of the radial component can significantly alter the effective length of the compensating spacer to achieve thermal balance. As the radius of curvature increases, the effect is reduced. Table 7 summarizes the components, material properties and design lengths for this example.

Radius (mm)	50.000
y_c (mm)	12.000
α_G (ppm/°C)	7.20
α_M (ppm/°C)	23.6
α_S (ppm/°C)	5.40
ΔSAG /°C (mm)	1.280E-04

TABLE 6. Starting parameters to calculate the ΔSAG per °C.

Component	Material	Bulk CTE (ppm/°C)	Length (mm)	ΔL/°C (mm)
Lens	S-BSL7	7.20	5.539	3.988E-05
Spacer	Vespel SP-1	5.40	7.199	3.887E-04
			ΔSAG	-1.280E-04
Housing	6061	23.6	12.737	3.006E-04
		Expansion Difference		**0.000**

TABLE 7. Summary of the materials, dimensions and total differential expansion for the axial compensator design with radial effects. The ideal length of the compensating spacer in this case is 7.199mm. This value is considerably larger than the solution that does not include the radial effects.

In general, if the ratio of R/yc is larger than 40, the radial effect error will be 10% or less and either method can be used. Figure 17 shows the effect of radius on the ideal compensating spacer value using the example lens. The plot shows that as the lenses become more hemispherical, the SAG change increases dramatically. Likewise, Figure 18 shows a lens of constant radius of 50mm and the relationship of varying the yc height on the length of the ideal compensating spacer.

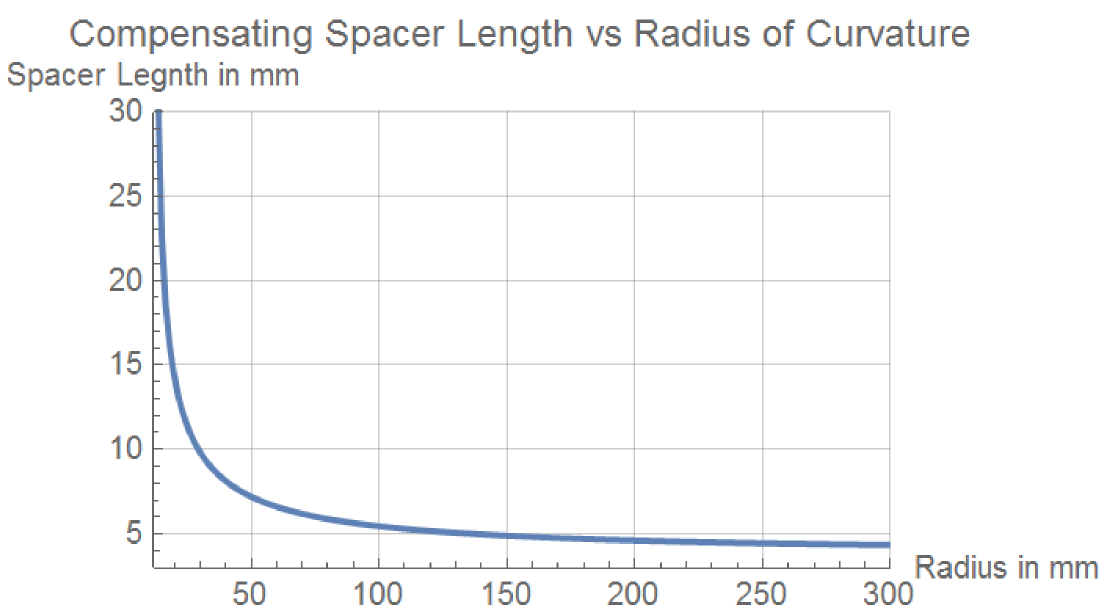

FIGURE 17. Compensator length vs radius of curvature. Small radii of curvature require a large length for compensation.

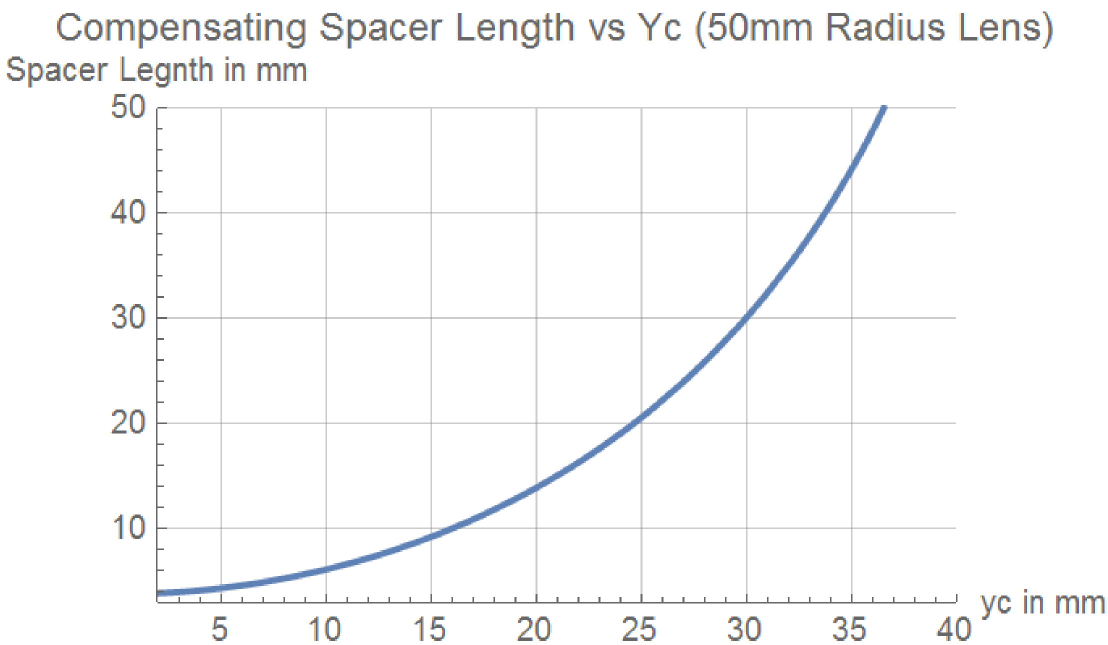

FIGURE 18. Compensator length vs the yc contact height. A large yc height requires a long compensating spacer.

An optical system of lenses that all have radii to yc ratios of 40 or larger is an unlikely scenario. A method to mitigate this effect would be to utilize a second spacer that interfaces with the lens, where this spacer has a lower CTE than the compensator or where the CTE is closely matched to that of the glass. Titanium is an excellent choice for this application as the CTE is 8.6 ppm/°C, a near perfect match for most optical glasses. By matching the CTE closely, the contribution from the ΔSAG effect can be dramatically reduced. There is an additional benefit to using an interfacing spacer between the compensator and the optical surface. Instead of the typical polymer compensator making the line contact, a stiffer material can be used instead.

An additional design consideration when evaluating and selecting compensating spacers is to be mindful of the material behaviors and the effect on the optical system. In particular, it is important to keep compensating spacers out of critical optical airspaces. A case study with a PTFE spacer used in between two lenses showed some hysteresis over temperature excursions [10]. This airspace was attempted to be used for thermal focus compensation but proved to be problematic. For axial preload compensation, a small amount of hysteresis will only contribute to a small preload variation with temperature. In most cases, the initial preload required to support the lens will be much larger than this variation. As long as this compensating spacer is not influencing a critical airspace, there will be no adverse effects on the performance of the system.

Each application needs to be carefully considered before a decision can be made that an axial compensator would be a good choice. The advantage for these compensating spacers is the reduction or elimination of thermal changes in preload on the optic. Since the stress imparted into the optic is directly related to preload, these compensating spacers will reduce this effect. Stresses can have a negative impact on performance as the surface can de-figure and there can be a change in the wavefront as light propagates through the lens surfaces. In addition to reducing the stress variation over temperature the compensating spacer also reduces the concerns of lens shifting at elevated temperatures. This effect is particularly pronounced in lens based imaging systems where calibration or distortion mapping of the lens is performed. Even very small shifts in the lens radial positions can degrade the effectiveness of the mapping.

Although the use of thermally compensating spacers appears to be a very useful design method it does have some drawbacks to their use and implementation. The most notable disadvantage is the length required to perform the compensation. These thermally balanced spacers can have a thickness that is quite large. This creates a long, broad surface where rays can strike at or near grazing incidence. These rays may originate from bright objects outside of the field of view where the scattered stray light rays have an opportunity to reflect and transmit unwanted energy onto the detector. Figure 19 shows a conceptual example of unwanted light rays reflecting off of the compensating spacer. Even relatively thin compensating spacers can pose a challenge for controlling stray light as many polymers used for such spacers can have a large percentage of light reflected in the specular direction. In some cases, materials can be chosen that work well mechanically as a compensating spacer but have some degree of translucency. These materials should be approached with extreme caution when considering their use in optical systems. These translucent spacers can collect and transmit light in unwanted ways resulting in reduced performance of the system.

The design of axial compensating spacers to mount lenses is one step on the path to producing a thermally balanced lens. The other contributions to be considered are radial compensation and focal compensation, and will be addressed in the next sections.

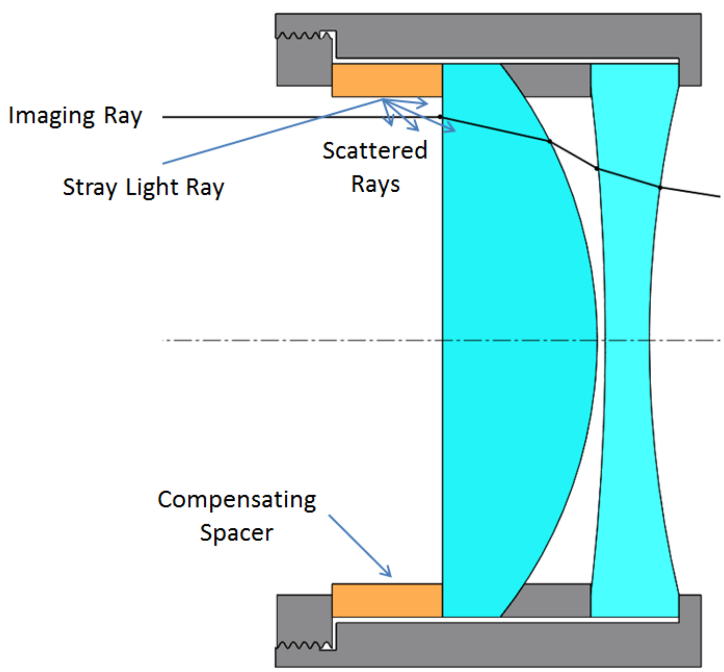

FIGURE 19. Potential optical issues using an axial compensator where stray light rays have an opportunity to scatter on the large broad surfaces of the spacer.

6. Radial Compensator Design

Similar to the approach with the axial compensation, there are methods to mitigate the differential radial dimensional changes with temperature. In cases where the use of a retainer or spacer is not possible, or where the design merits a radial mounting contact, the design can still be thermally balanced. Furthermore, the axial compensation design can be combined with a radial compensation design to produce an extremely robust lens mount.

During thermal excursions, the radial gap between the lens element and the housing will change if the there is a difference in CTE of the components. This gap can be calculated by using Equation 22. The sign of the gap change is depended on the materials for the lens and the housing. Lens housings with a higher CTE than the optical element will see an increase in the gap at elevated temperatures and a reduced gap at lower temperatures. Figure 20 shows a nominal radial gap during assembly and an increased radial gap at elevated temperature for a glass lens element and aluminum housing. A tight radial gap is a method for constraining the decenter of optical elements but can present a threat to performance or the survival of the optic with changes in temperature. For the case of a glass element and an aluminum barrel, a decrease in temperature will result in contact of the housing to the rim of the lens and the development of stress. This stress both impacts the optic as well as the housing. The magnitude of the radial stress, σ_R, in the optic can be calculated by Equation 23, where K4 and K5 are shown in Equation 23a and 23b respectively. The term Δr in Equation 23b needs to be carefully considered when the value exceeds $D_G\Delta T(\alpha_M-\alpha_G)/2$. When this occurs, there is no longer contact between the lens element and the housing and no stress is developed [5]. This applies to both σ_R and σ_M. The stress in the housing, σ_M, can be calculated with Equation 24. This is the radial stress in the housing wall.

$$\Delta GAP = (\alpha_M - \alpha_G)\left(\frac{D_G}{2}\right)\Delta T \qquad \text{Eq. (22)}$$

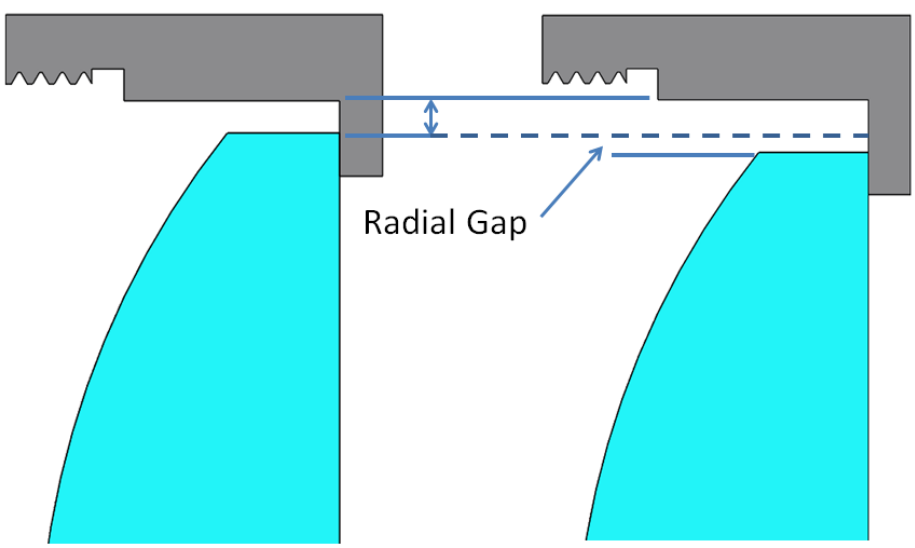

FIGURE 20. Cross-section showing the increase in radial gap for a glass lens and an aluminum housing at elevated temperature.

$$\sigma_R = -K_4 K_5 \Delta T \qquad \text{Eq. (23)}$$

$$K_4 = \frac{\alpha_M - \alpha_G}{\frac{1}{E_G} + \frac{D_G}{2E_M t_C}} \qquad \text{Eq. (23a)}$$

E_G = Modulus of elasticity (glass)
E_M = Modulus of elasticity (metal)
D_G = Diameter of the lens
t_c = Radial thickness of the housing wall
α_M = CTE (metal)
α_G = CTE (glass)

$$K_5 = 1 + \frac{2\Delta r}{D_G \Delta T(\alpha_M - \alpha_G)} \qquad \text{Eq. (23b)}$$

Δr = radial clearance (nominal gap)

$$\sigma_M = \frac{\sigma_R D_G}{2t_C} \qquad \text{Eq. (24)}$$

One method to reduce or eliminate the change in the radial gap with temperature is to use a bonding material between the housing and the lens element. Typically this bonding material is RTV (room temperature vulcanizing rubber). RTV566 is an RTV that has been successfully used for athermalizing optical elements with a CTE of 200 ppm/°C. Figure 21 shows a cross section of a lens element and housing where the gap has been filled with RTV. The optimum gap can be calculated using Equation 25 [11]. In cases where the gap is very large, such as a large diameter element or components with a high differential CTE, a pre-cured pad of RTV can be placed in the gap and the surfaces can be bonded with a small amount of additional RTV.

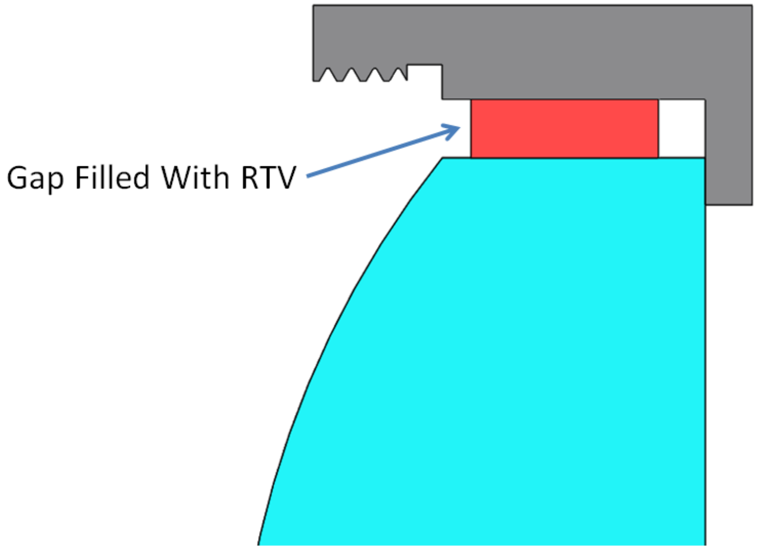

FIGURE 21. Cross-section of a lens where the radial gap has been filled with RTV.

$$t = \frac{D_G}{2}\frac{(\alpha_M - \alpha_G)}{(\alpha_R - \alpha_M)} \qquad \text{Eq. (25)}$$

α_M = CTE (metal)
α_G = CTE (glass)
α_R = CTE (RTV)
D_G = Diameter of the lens

An area to be careful when using or selecting RTV is that these materials can have a Poisson's ratio between 0.4 and 0.5. The result of this, cited by Yoder, shows that the bulk CTE may be off by a factor of 2.5 to 3.0 [5]. Instead of using the bulk CTE, the effective CTE is used. Using the 2.5 factor of the bulk CTE is a reasonable back of the envelope approximation for the effective CTE [5]. An enhanced version of calculating the thermal bond gap was developed at Lockheed Martin and is shown by Equation 26 [5]. The Poisson's ratio of the RTV is used in this equation to determine the appropriate radial gap. In this case, the bulk CTE can be used as the Poisson's ratio is included in the formula to account for the difference of the effective CTE. Generally, the difference between the two equations is small when using the effective CTE in Equation 25, so it can be used as a good and fast approximation [5].

$$t^* = \frac{\frac{D_G}{2}(1-\nu_R)(\alpha_M - \alpha_G)}{\alpha_R - \alpha_M - \nu_R(\alpha_G - \alpha_R)} \qquad \text{Eq. (26)}$$

ν_R = Poisson's ratio of the RTV

Another method for athermalizing the radial gap is with the use of a compensating radial spacer [1]. Equation 26 can be utilized with a polymer instead of the RTV. The polymer is made in a way to fit between the rim of the optic and the inside diameter of the housing. Figure 22 shows a recreation of the spacers used in the JPL MISR lens [1]. An important aspect to this method is that the ideal thickness calculated will be much larger than the RTV solution. This is simply due to many polymers having a lower CTE than RTV. The extra thickness may not be the best choice in cases where the volume claim of the lens housing is limited or other constraints are placed on the system geometry. In order to assemble the radial compensating spacer, there needs to be some clearance between the lens and the inside diameter of the spacer, as well as clearance between the outside diameter of the spacer and the inside diameter of the housing.

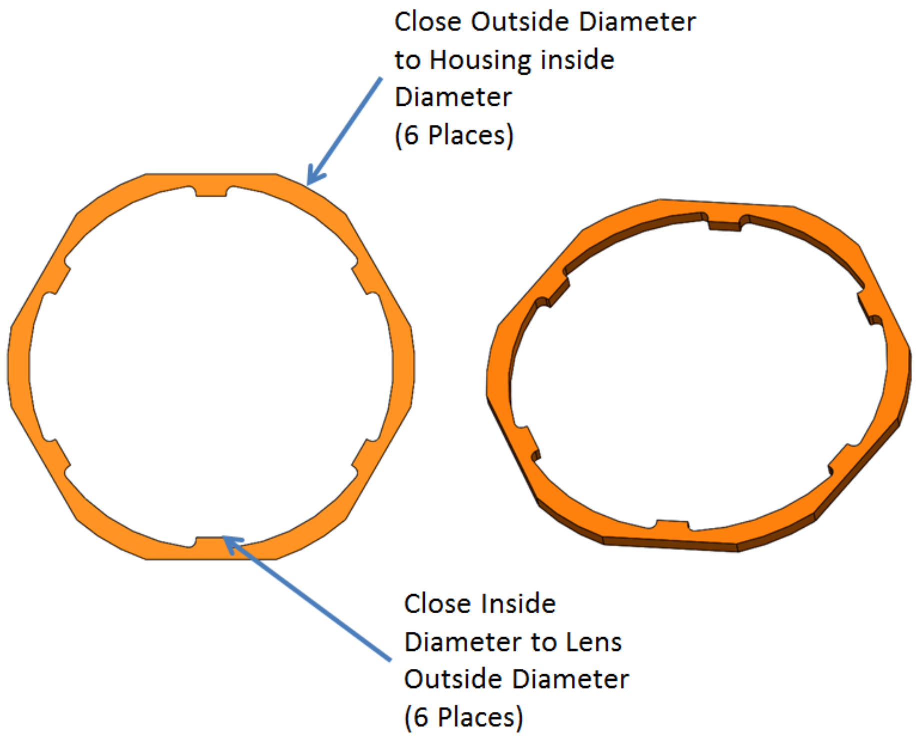

FIGURE 22. A recreation of the radial spacers used in the JPL MISR lens.[1]

6.1 EXAMPLE: Radial Compensator

A design example can be explored based on the radial thermal balancing approaches in this section. Consider a 25mm diameter lens made from Ohara S-BSL7 that is to be radially mounted in a lens housing. Using Equation 25, the ideal thickness of RTV can be found using both the bulk and effective CTEs. Alternatively, Equation 26 can be used to solve the radial RTV gap using the bulk CTE. The difference between Equation 25 with the effective CTE and Equation 26 with the bulk CTE is negligible, but it is important to check as certain situations or materials may give different results. Table 8 summarizes the design parameters and Table 9 summarizes the values for the two different approaches for the RTV thickness. Note that the bulk CTE with Equation 26 would be appropriate for materials with a Poisson's ratio less than 0.4.

Component	**Material**	**Bulk CTE (ppm/°C)**	**Eff. CTE (ppm/°C)**
Lens	S-BSL7	7.20	
Housing	6061 Aluminum	23.6	
RTV	RTV566	2.00	5.00

TABLE 8. Summary of the materials and CTE values for the 25mm diameter lens used in the example. The RTV is assumed to have a Poisson's ratio of 0.43 and a factor of 2.5 was used to determine the effective CTE.

Ideal RTV Thickness (mm)	
Method 1 Bulk CTE	1.162
Method 1 Eff. CTE	0.430
Method 2 Bulk CTE	0.451

TABLE 9. Summary of the various methods used in the example to calculate the ideal RTV thickness. Method 1 using the effective CTE and Method 2 using the bulk CTE are nearly identical. For materials with a Poisson's ration larger than 0.4, the use of Method 1 with the bulk CTE is not recommended.

The advantages of radial compensation are the reduction in stress on the optic in cases where the housing could contact the lens rim. For lenses that are mounted solely by radial bonding, such as space based lens systems, the RTV pads provide a significant amount of shock resistance between the housing and the lens element. This can be advantageous for optical lens systems that may experience pyroshocks from launch vehicles. Additionally, radial bonding can aid in containing the lenses from moving radially over temperature and shocks. For systems that are sensitive to lens decentration movements, radial constraint is a desirable design property.

The disadvantages of the radial compensation methods are the size requirements to accommodate the various design methods. In cases where the diameter of the lens barrel is constrained, there may not be a solution without cutting into the clear aperture margin of the lenses or thinning of the lens barrel wall thickness. The use of the radial spacer may also pose some issues with properly constraining the lens from radial movements. By design, a small amount of clearance is likely needed for assembly reasons. This small radial gap, perhaps on the order of 10-25 microns, would allow the lens element to decenter. In sensitive optical systems, this amount of decentration is enough to have a noticeable effect on performance.

7. Compliant Mounting Methods and Design Considerations

There are some additional methods for mounting lenses to accommodate the differential expansion over temperature. These methods include the use of complaint or spring members that interface with the lens and provide a mechanical means to alleviate the dimensional changes that can occur over temperature excursions [5]. These compliant components provide the compensation but do not function as a hard mount like the compensating spacer solution described in the sections above. Here a spring or otherwise compliant component is placed between the lens and the retainer or housing. These compliant components can be used for both axial and radial compliance. The simplest method for accomplishing this is the use of an axial spring. This can be a wave spring, Belleville disc spring or spring flexures. Figure 23 shows a lens with a Belleville type disc spring and a retainer.

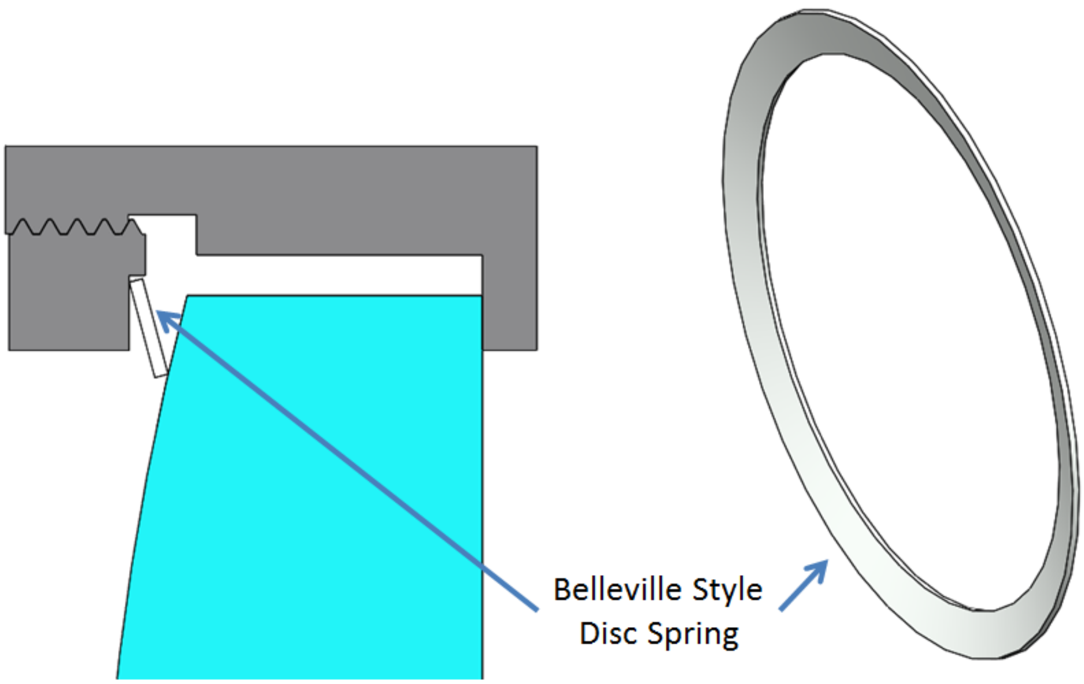

FIGURE 23. Cross-section of a lens showing the use of a Belleville type disc spring providing axial compliance against the lens surface.

Rather than add a compliant spring between the lens and the retainer, the compliance can be designed directly into the retainer. Figure 24 shows an example of a retainer with axial compliance.

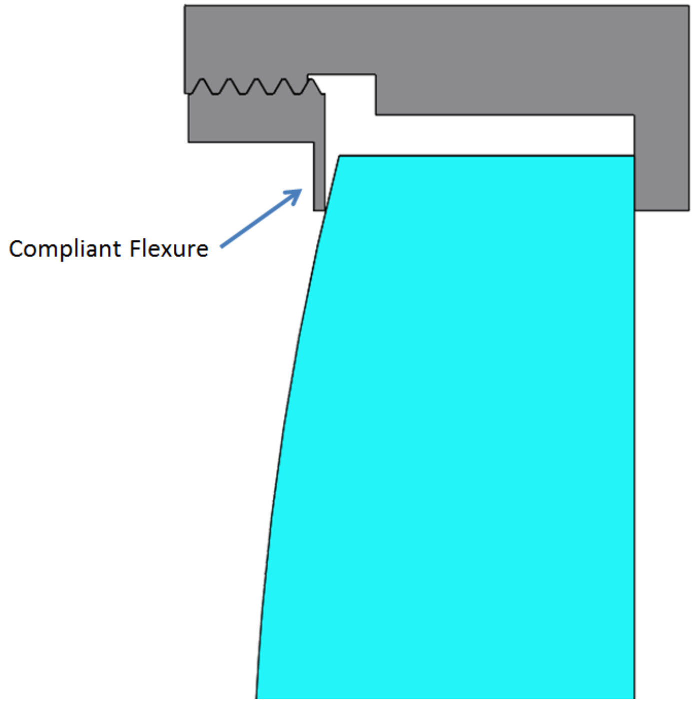

FIGURE 24. Cross-section of a lens showing a diaphragm flexure integrated into the threaded retaining ring to provide axial compliance.

In addition to an axially complaint design, the radial differential expansion with temperature can also be accommodated with a spring style design. One such method is the use of flexures to support the lens in the radial direction [5]. Figure 25 shows a lens supported radially with leaf style flexures.

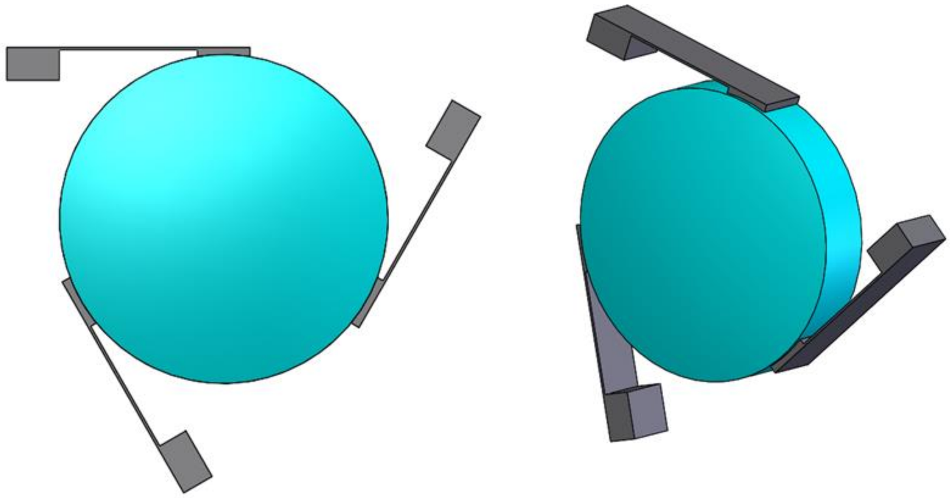

FIGURE 25. Flexures used for radial compliance.

Providing compliance to a lens mount has many advantages. In addition to accommodating thermal changes, the compliant mounting method can also tolerate dimensional errors in manufacturing. Since the spring force is set during assembly, a component with a modest dimensional error is unlikely to change the assembly result for a desired preload.

Some caution should be exercised when considering spring compliant mounts for high shock environments. These mounts can certainly perform well, but if not properly sized and analyzed, they can result in damage to the optic. For high accelerations, the weight of the optic can compress the compliant spring members and potentially impact the optic back into its mount. Another issue with spring loads, if they are performed by a few discrete members, is that they can have uneven loading due to dimensional differences during manufacture or assembly. In these cases, the loading can be uneven and can potentially exhibit some unexpected positional changes over thermal excursions.

8. Thermal Focus Compensation

Thermally balancing the mechanical mounting and constraint for the lenses is important for the performance of individual elements. However, the system as a whole may exhibit issues with temperature changes. Specifically, the image plane of the system may change in position over temperature excursions due to the thermal change in focus described in Section 3. The thermal change in focus is the result of the combined dn/dT for each element and the dimensional airspace changes between the lenses over temperature. This can be characterized using optical design software and is assumed to be complete for the opto-mechanical engineer to start the process of thermally balancing the mechanical elements.

The most pertinent and useful information of change in focus for the opto-mechanical engineer is the flange focal length (FFL) over temperature. Figure 26 shows a lens assembly and the definition of the flange focal length, where the flange is the structure of the lens assembly that attaches to the structure of the focal plane array. The FFL change with temperature is based on the particular optical design and the individual dn/dT of each optical element. It is possible to have a negative FFL change with temperature or a positive FFL change with temperature and this depends on the particular optical design.

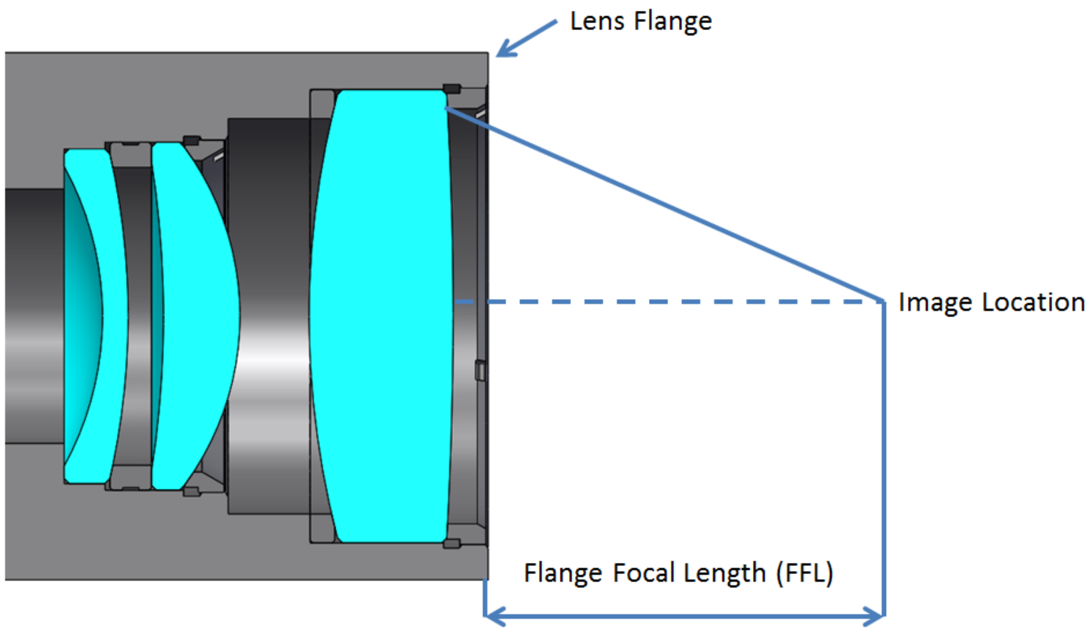

FIGURE 26. Cross-section of a lens assembly showing the definition of the flange focal length.

Once the change of focus is determined from the optical design, the opto-mechanical engineer can start to look at methods for compensating the dimensional change. The methods for thermal balancing the focus shift with temperature depend on the sign of the FFL change with temperature. For the positive case, where an increase in temperature lengthens the FFL, a spacer with an appropriate CTE and length can be used to compensate the dimensional shift. For the case of the negative FFL change with temperature, a more complex approach is required. Figure 27 shows the negative FFL change with temperature where an increase in temperature shortens the FFL. One such method for the negative FFL case is the use of materials with different CTEs that are configured in a manner to provide differential expansion that matches the negative flange focal length change. This method is typically designed by using nested barrels of dissimilar materials. Figure 28 shows the conceptual approach to nesting materials with different CTEs. Figure 29 shows the resulting dimensional changes for both low and high temperature cases.

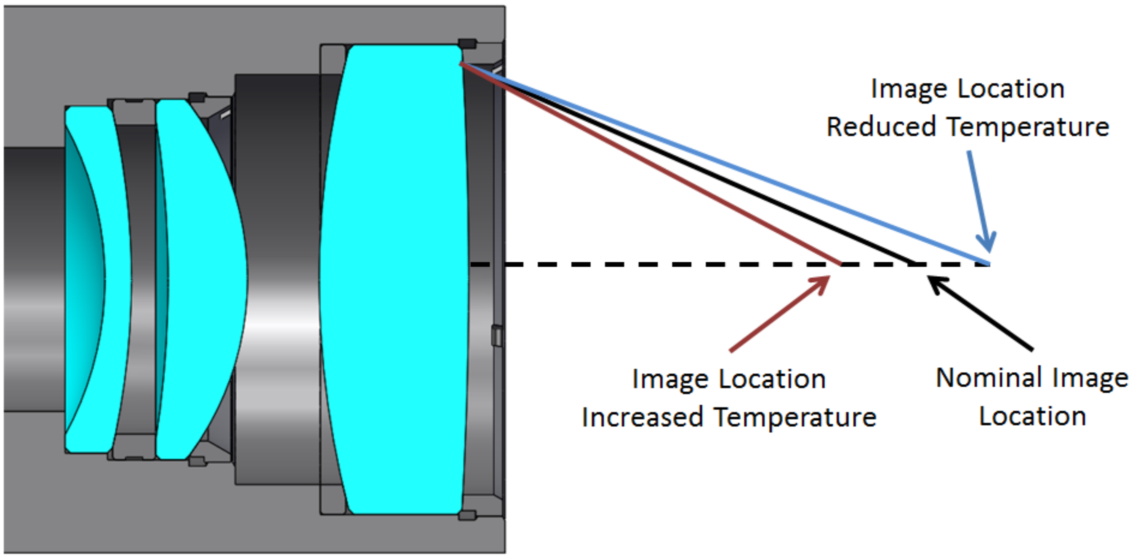

FIGURE 27. Cross-section of a lens assembly showing the changes of the image location with both elevated and reduced temperature. This is the negative case where the FFL of the lens is shortened at elevated temperature.

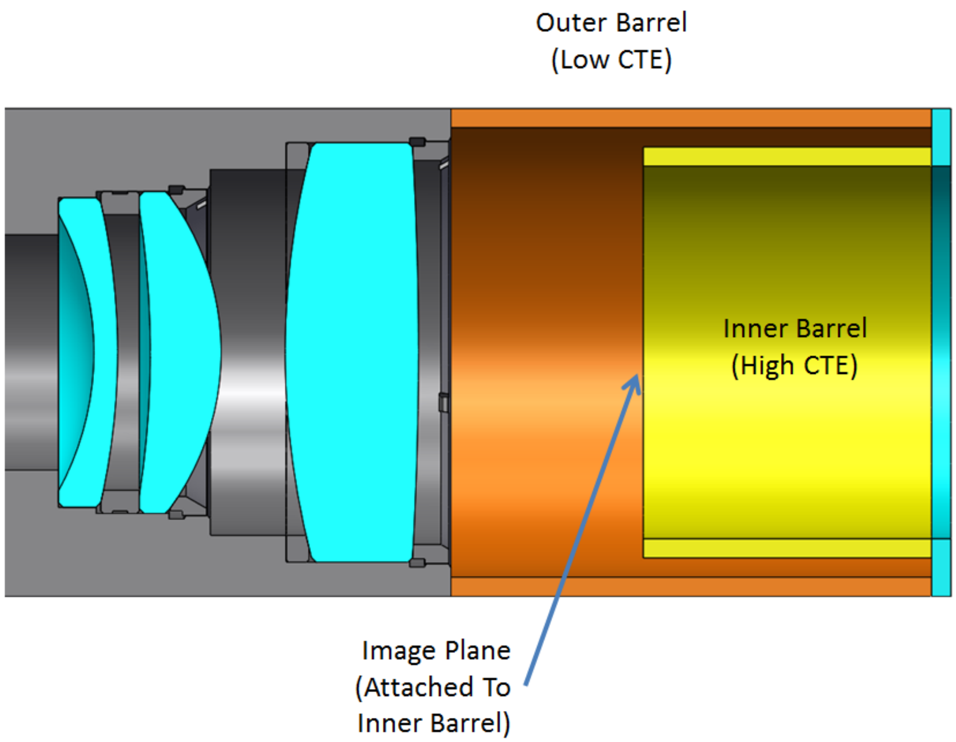

FIGURE 28. Cross-section showing the conceptual approach for a nested barrel thermal focus compensator.

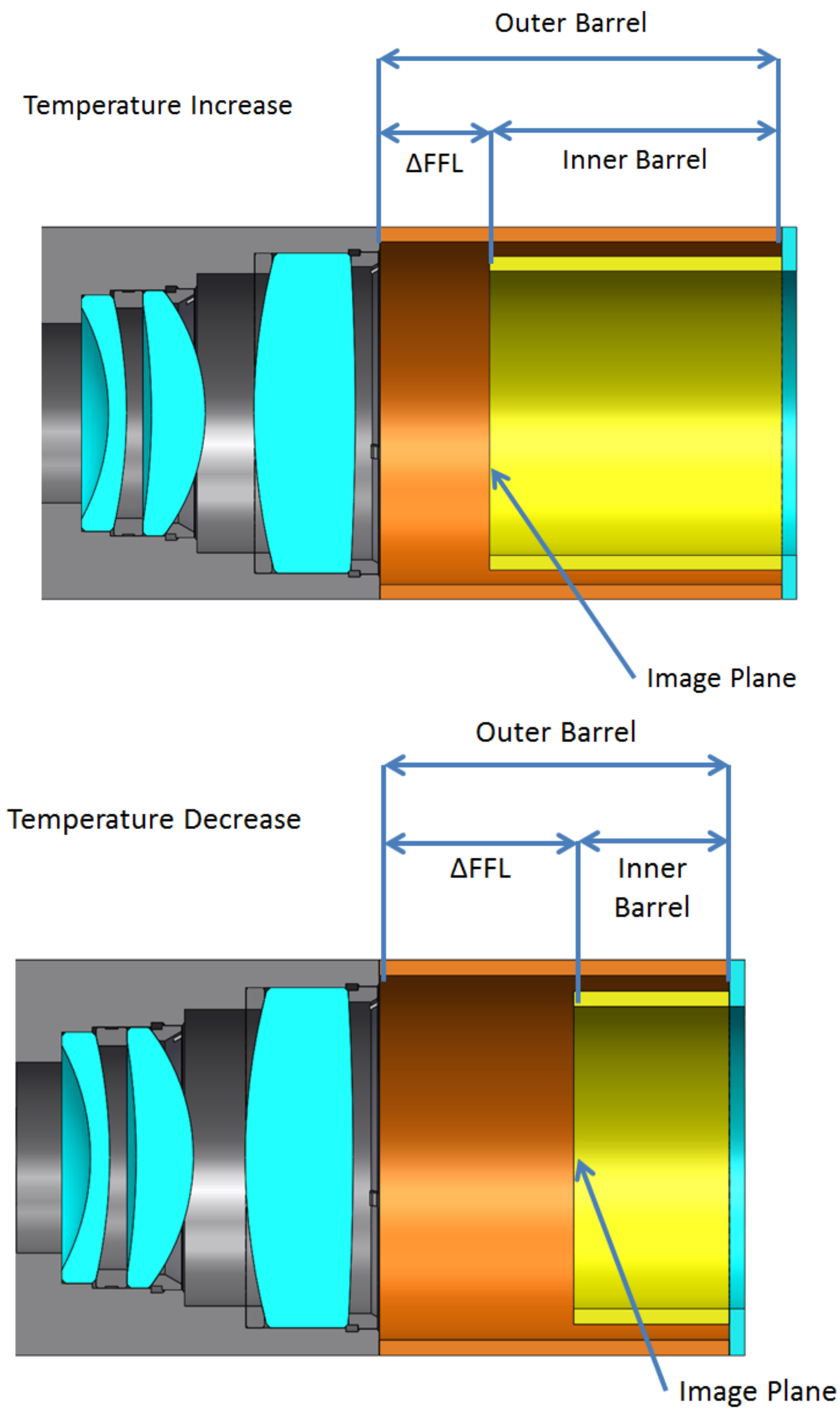

FIGURE 29. Cross-section showing the differential dimensional changes for the nested thermal focus compensator at both high and low temperature.

Depending on the configuration of the lens design or other mechanical volume limitation, it may not be possible to use the nested barrel method to achieve thermal balance of the focal shift with temperature. In these cases it may be valuable to check the optical design for the possibility of adding a refocusing group. A focusable group can be motorized or it can be thermally metered in a similar fashion to the nested barrel approach.

Some design considerations for thermally balancing the focus change are the structural stability and the effect of tolerancing on the compensator elements. The nested barrel approach may be susceptible to undesired deviations during vibrational inputs. Even though round barrels are quite stiff, the effective length of the nested configuration can lower the overall modal frequency and pose a risk to image blur in certain situations. The tolerancing is important to analyze as the flange focal length, nested compensation and the df/dt can all be affected by small dimensional inaccuracies. Incorporating shims or other axial adjustments would be wise to allow the nested compensation barrels to be tuned to each specific build.

9. Thermal Gradient Considerations

The methods described to design thermally balanced lens mounting has assumed a homogeneous steady-state temperature change. This is rarely the case in reality and non-uniform thermal distributions need to be considered when evaluating the merits of a design approach. These non-uniform thermal distributions are referred to as thermal gradients. A thermal gradient means that the mechanical components, the optical elements and other parts of the system will be experiencing different temperatures. In optical systems, thermal gradients can sometimes be preferentially oriented in the axial direction, preferentially oriented in the radial direction or in some combination of the two. This temperature distribution can be found by finite element analysis and can give insights into how the system will change over temperature. An extreme type of thermal gradient is known as a thermal shock. Here an optical system at some temperature is exposed to an extreme temperature change very rapidly. Thermal shocks can be so severe that the internal strain in an optical element can cause the glass to fracture.

Closed form solutions for thermal gradient problems are extremely limited and only apply to simplified geometric conditions. The most appropriate way to analyze the effects of a thermal gradient on a particular design is to use the finite element method. However, the opto-mechanical engineer can make some careful material choices prior to the finite element analysis that can provide some advantages for a system experiencing thermal gradients. The parameters for comparing and selecting materials are the thermal conductivity (K), the coefficient of thermal expansion (α) and thermal diffusivity (D). Thermal diffusivity describes how long it takes for heat to spread out through a material [11]. Choosing materials with a high thermal diffusivity can help a design be more predictable with the profile of the gradient and thus make it easier to mitigate the effects. Thermal conductivity describes how resistive a material is to a change in temperature. The methods for thermally balancing a lens system described in the sections above can still be effective even in the presence of thermal gradients. However, each design must be carefully modeled and analyzed to ensure that the result will be successful.

10. Thermal Properties of Exotic Materials

When considering how to thermally balance an optical system, materials are typically paired to produce a differential thermal expansion in the desired direction. Since the vast majority of practical materials have a positive CTE, this method requires some considerable dimensional lengths to accomplish the thermal balancing. Mathematically, it would be desirable to have a material that has a negative CTE, thus it could be directly applied without the complication of pairing. Until recently, these exotic negative CTE materials have been a topic of research but have not made it to be readily used commercially. Allvar, founded in 2014, is a company that specializes in negative CTE metals that can be readily machined and used by industry.

Allvar Alloy 30 is a titanium based alloy that features a significantly high negative CTE of -30 ppm/°C. Figure 30 shows a plot of the percentage strain vs temperature for Allvar Alloy 30 and various other materials. Table 10 shows some properties of Allvar Alloy 30 as well as some traditional metallic materials for comparison [12]. Normal materials exhibit a positive slope and thus have a positive CTE. Alllvar Alloy 30 exhibits a large negative slope. This material can be successfully used for compensating a focal shift with temperature where the flange focal distance shortens with an increase in temperature. The advantage for using a negative CTE material for thermal balancing of focus is that the design can become more compact. A simple spacer of Allvar Alloy 30 can be designed and placed between the lens flange and the focal plane.

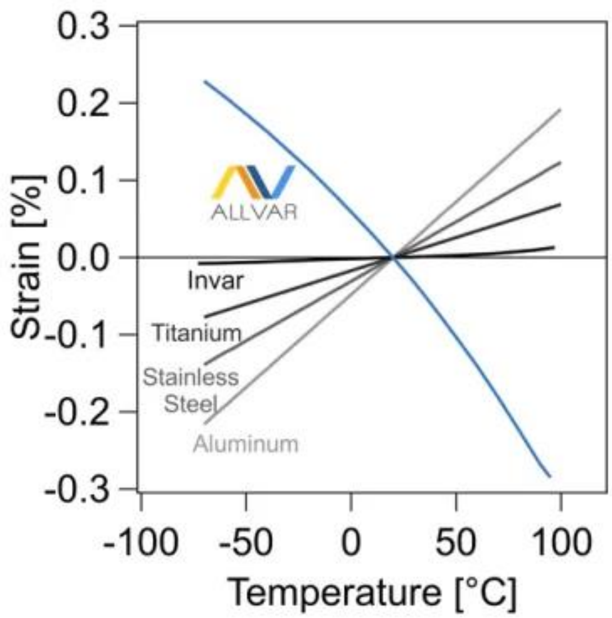

FIGURE 30. Plot showing the strain vs temperature curve of Allvar and other common materials. [12]

Property	Units	ALLVAR Alloy	Invar	304 Stainless Steel	6061 Aluminum	Titanium 64
CTE Range @20°C	(ppm/°C)	-30	1.6 to 6	17.3	23.6	9
Max Operating Temperature	(°C)	100	200	870	120	540
Yield Stress	(MPa)	710	276	215	55	828
UTS	(MPa)	750	448	505	124	895
Elastic Modulus	(GPa)	75	141	193	68.9	113.8
Density	(g/cc)	5.08	8.1	8.0	2.7	4.42
Thermal Conductivity	(W/m·K)	6.2 - 8.7	10.15	16.2	180	6.6

TABLE 10. Summary of the properties for Allvar Alloy 30 and other common materials for comparison. [12]

Careful application of negative CTE materials can be used to enable an optical system to be thermally balanced. These exotic materials do have an expense associated with them, but can be a good option for compact designs. Also, this material would only be a good choice for systems expecting to see temperatures below 100 °C.

11. Closing

The methods presented for thermally balancing the mounting of refractive elements and balancing the thermal change of focus can improve the performance of optical systems during thermal excursions. Compensating spacers can reduce or eliminate the changes in axial loads placed on lens elements and reduce stress increases imparted onto the optic. Thermal balancing can also ensure that the focal shifts with temperature are compensated so that the imaging performance is preserved over wide temperature changes. Even if a system is not likely to experience thermal changes, the design methods described enable low stress mounting to achieve high performance optical systems.

12. Resources

1. Ford, V.; White, M.; Hochberg, E.; McGown, J., *Optomechanical Design of Nine Cameras for the Earth Observing Systems Multi-Angle Imaging Spectral Radiometer, TERRA Platform*, Proceedings of SPIE 3786, 1999.

2. Karow, Hank H., *Fabrication Methods For Precision Optics*, John Wiley & Sons, Inc., 2004.

3. Ohara Corporation, "*https://www.oharacorp.com/catalog.html*", Accessed April 2021.

4. Doyle, K.; Genberg, V.; Michels, G., *Integrated Optomechaincal Analysis*, 2nd Edition, SPIE, 2012.

5. Yoder, Jr., Paul,; Vukobratovich, D., *Opto-Mechanical Systems Design*, 4th Edition (Volume 1), CRC Press, 2015.

6. Schwertz, K.; Burge, J., *Field Guide to Optomechanical Design and Analysis*, FG26, SPIE Field Guides, 2012.

7. Pepi, John W., *Opto-Structural Analysis*, SPIE, 2018.

8. NASA Outgassing Data for Selecting Spacecraft Materials, "*https://outgassing.nasa.gov"*, Accessed March 2021.

9. Boedecker Plastics, Inc., "*https://www.boedeker.com/Industries/Industry-Landing/High-Purity*", Accessed April 2021.

10. Fischer, R.; Tadic-Galeb, B; Yoder, Jr., P., *Optical Systems Design*, 2nd Editions, Mcgraw-Hill, 2008.

11. Kasunic, Keith, *Optomechanical Systems Engineering*, John Wiley & Sons, Inc., 2015.

12. Allvar, "*https://allvaralloys.com/what-is-negative-coefficient-of-thermal-expansion*", Accessed April 2021.